Characterization of Self-Assembling Quinoline-Based Foldamers by Fluorescence Anisotropy

by

Jingqi Wang

A thesis

presented to the University of Waterloo

in fulfilment of the

thesis requirement of the degree of

Master of Science

in

Polymer Chemistry

AUTHOR'S DECLARATION

I hereby declare that I am the sole author of this thesis. This is a true copy of the thesis, including any required final revisions, as accepted by my examiners.

I understand that my thesis may be made electronically available to the public.

Abstract

Foldamers represent a family of synthetic macromolecules which, like their biological counterparts, are able to adopt a well-defined conformation in solution. Oligoquinoline-carboxamides (Q_n) are a group of foldamers that adopt a helical conformation in solution. A series of Q_n foldamers were prepared by chromatography-free large-scale synthesis and segment-doubling strategy. The C-terminal ester group of the Q_n foldamers could be hydrolyzed to yield acid-functionalized foldamers (Q_nA) which could self-assemble into larger (($Q_nA)_2$-Na) complexes by metal coordination with a sodium cation. Moreover, the addition of a *bis*-acid functionalized tetramer (AQ_2PQ_2A) to a solution of ($Q_nA)_2$-Na complexes resulted in insertion oligomeric products. To characterize these complexes in solution, both Q_n and Q_nA were end-labeled with an oligo(phenylene vinylene) dye (OPV) at their *N*-terminus via a rigid amide bond to yield the OPV-Q_n and OPV-Q_nA fluorescent equivalents. OPV was used to conduct time-resolved fluorescence anisotropy (TRFA) measurements on the OPV-Q_n and OPV-Q_nA foldamers, the (OPV-$Q_nA)_2$-Na complexes, and the OPV-Q_n-Na-$(AQ_2PQ_2A)_n$ oligomers. Analysis of the TRFA of the OPV-Q_n foldamers yielded the rotational time (ϕ) of the fluorescent species, which was found to reflect the hydrodynamic volume (V_h) of the foldamers. The straight line obtained by plotting ϕ as a function of the number of (quinoline) units (NUs) demonstrated that the foldamers behaved in solution as rigid cylinders for all lengths examined. The linearity of the ϕ-vs-*NU* plot was employed as a calibration curve against which the rotational time of the Q_nA-complexes could be compared. Within experimental error, the rotational time of a Q_{n+m} complex was found to equal the sum of the rotational times obtained for Q_n and Q_m. This result suggests that the complexation of two acid-functionalized oligoquinoline foldamers in solution generated a fully stacked foldamer with a NU equal to the sum of the NUs of its constituting elements. Hetero-complexes between OPV-Q_8A

and $Q_{16}A$ were also produced by adding a 10-fold excess of $Q_{16}A$ to an OPV-Q_8A solution. Complexation was demonstrated by the ϕ value of the mixture, that equaled that of an OPV-Q_{24} foldamer. Dilution experiments on a solution of OPV-Q_8A-Na-$Q_{16}A$ complexes led to the dissociation of the complexes into their OPV-Q_8A and $Q_{16}A$ constituting elements, as evidenced by the progressive decrease in ϕ from the value obtained for OPV-Q_{24} to that of OPV-Q_8 upon decreasing foldamer concentration. Similarly, the addition of increasing amounts of AQ_2PQ_2A to a solution of OPV-Q_8A in chloroform resulted in an increase in ϕ, demonstrating the formation of complexes between OPV-Q_8A and AQ_2PQ_2A until ϕ reached a plateau for large OPV-Q_8A/AQ_2PQ_2A molar ratios. In the plateau region, the rotational time of the oligomeric complexes generated from OPV-Q_8A and AQ_2PQ_2A stabilized by isobutyl or hexyl side chains was equal to that of an OPV-Q_n foldamer with *n* equal to 24 or 30, respectively. The apparent absence of further polymerization, evidenced by the constant ϕ value reached for high OPV-Q_8A/AQ_2PQ_2A molar ratios, was attributed to aggregation of longer complexes and their precipitation. This study represents the first example in the scientific literature where TRFA was applied to characterize the NU of helical self-assembling foldamers in solution.

Acknowledgements

I want to express my sincerest gratitude to several people who helped me and encouraged me to carry out this project.

First, I want to thank my supervisor at UW, Prof. Jean Duhamel, who provided me with the rare opportunity to deeply understand the field of chemistry and a chance to study in Europe. He not only taught me polymer science and fluorescence, but also the thinking process involved when doing research. He has really played an important role in my professional development. Also, I want to thank Dr. Victor Maurizot and Dr. Jinhua Wang from the laboratory of Dr. Ivan Huc in France, who trained me for the synthesis of foldamers with patience and erudite knowledge. Without them, I could not have prepared the foldamers used in my project. They also contributed to the nice experience I had in Bordeaux. Then I would like to thank all my collaborators and friends in the Huc and Duhamel laboratories. They have offered me awe-inspiring opportunities to study new research fields and expand my view of science.

Last but not least, I sincerely thank my parents and family for supporting me as I went abroad to pursue my personal interest in Chemistry. I can always feel their care and support.

Table of Contents

List of Figures

List of tables

List of schemes

List of abbreviations

Abs	Absorption
AQ_2PQ_2A	Pentamer with a pyridine at its center, flanked by two quinoline dimers terminated at both ends with a carboxylic acid
β_A	Angle between the absorption dipole moment of the dye and the main axis of the helix
β_E	Angle between the emission dipole moment of the dye and the main axis of the helix
D	Diameter of helical foldamer
$D_{//}$	Diffusion coefficient for the tumbling of a symmetric top macromolecule around its main axis of symmetry
$D_{\perp}$	Diffusion coefficient for the tumbling of a symmetric top macromolecule around its secondary axis of symmetry
D_w	Diffusion coefficient for wobbling of OPV around the main axis of a helical foldamer
DP	Degree of polymerization
Δh	Helical rise per quinoline residue
E	Molar extinction coefficient
$F_{OPV}(\lambda)$	Normalized fluorescence intensity of OPVA
ϕ	Rotational time
Φ	Quantum yield
G	G-factor
η	Solution viscosity
K	Equilibrium constant
I_o	Fluorescence intensity at t=0
I_F	Fluorescence intensity
$I_{XY}(t)$	Fluorescence intensity acquired with an excitation light polarized in the X-orientation and an emission polarized in the Y-orientation where the X and Y-orientations can be horizontal (H), vertical (V), or at the magical angle (M).

κ^2	Orientation factor describing the relative orientation in space of the transition dipoles of the donor and the acceptor
L	Length of a symmetric top macromolecule along its main axis of symmetry
$\vec{\mu}_D$	Emission dipole moment of the donor
$\vec{\mu}_A$	Absorption dipole moment of the acceptor
N	Refractive index
N_A	Avogadro number
NU	Number of quinoline units in an oligoquinoline foldamer
N	Flory exponent
OPV	Oligo(phenylene vinylene)
OPV- Q_nA	OPV-labeled foldamer acid
OPV-Q_n	OPV-labeled foldamer ester
P	Aspect ratio ($p=L/d$) of symmetric top macromolecules
Q_n	Quinoline-based aromatic oligoamide foldamer with n units
Q_nA-Na-Q_mA	Foldamer complex between Q_nA and Q_mA formed via Na^+ coordination
Q_n-CO_2H	Acid-functionalized Q_n
Q_n-$COCl$	Acid chloride-functionalized Q_n
Q_n-NH_2	Amine-functionalized Q_n
θ_A	Angle between the absorption dipole moment of the acceptor and the vector joining the donor to the acceptor
θ_D	Angle between the emission dipole moment of the donor and the vector joining the donor to the acceptor
R	Steady-state anisotropy
$r(t)$	Time-resolved fluorescence anisotropy
r_o	Anisotropy at time t=0
R	Universal gas constant
R_o	Förster radius

R_h	Hydrodynamic radius
SSF	Steady-state fluorescence
T	Time
T	Absolute temperature
TRF	Time-resolved fluorescence
τ_o	Natural lifetime of OPV
τ_n	Decay times with n =1, 2, and 3
V_h	Hydrodynamic volume
ξ	Angle between the projection of the absorption and emission dipole moments in the plane perpendicular to the main axis of the symmetric top macromolecule.

Chapter 1

Introduction

1.1 Background

Foldamers are artificial oligomers designed to fold in solution via non-covalent intramolecular interactions.[1,2] Folding of these linear macromolecules is inspired from natural biomacromolecules such as peptides, oligonucleotides, or oligosaccharides and uses comparable types of interactions to lead to similar molecular architectures such as helices, sheets, or loops. The obvious parallels that exist between foldamers and biological macromolecules in terms of conformation suggest that foldamers could be designed to perform many of the functions conducted by biological macromolecules in nature.[3,4] However and contrary to nature, chemists are not limited by the bioavailability of natural building blocks such as amino acids, nucleobases, or sugars but can expand the scope of monomers used in foldamer preparation to all kinds of chemically accessible units.[5] This diversity may give access to new functions and usages remote from those commonly observed in nature, such as in molecular electronics[6–8] or in the nanoengineering field [9–11].

In that context, foldamers based on aromatic quinoline oligoamide backbones were designed to fold into helical architectures stabilized by intramolecular hydrogen bonds and aromatic stacking.[12] Recent synthetic developments have allowed the preparation of nanometer-sized objects, whose length scale and intrinsic conducting properties make them interesting as building blocks for materials science applications and for molecular electronics, respectively.[10] Furthermore, the preparation and characterization of dimer and polymer complexes obtained through complexation by metal coordination of different oligoquinoline foldamers, terminated at one or both ends with a carboxylate anion, also provide a new method to prepare longer helical

strands. However, these synthetic developments also brought to the fore a dearth of analytical techniques to characterize the overall dimensions of such large macromolecular constructs in solution.

By and large, single crystal X-ray diffraction (SCXRD) is the technique of choice to characterize the conformation of foldamers in the solid state.[13] Unfortunately, crystal packing forces are also known to induce conformations in the solid state that might not be observed in solution for a same macromolecule, and complementary solution studies by NMR or circular dichroism are necessary.[14–16] For instance, a combination of NMR spectroscopy and molecular modeling may provide a measure of the helical twist of a foldamer that can be used to predict its conformation in solution.[17,18] Enhanced or vibrational circular dichroism is able to assess the extent of folding of a foldamer in solution.[19–21] Changes in the UV-Vis absorption spectrum can indicate an increase in foldamer length.[8,22] However all these techniques characterize short range distances between residues in the foldamer and do not provide a sense of the overall dimensions of the foldamer in solution.

The common technique to probe the dimension of nm-scale macromolecules in solution is dynamic light scattering (DLS).[23] In the case of oligoquinoline foldamers, according to SCXRD, these constructs adopt a helical conformation with a 2.0 nm diameter and a 0.136 nm raise per quinoline residue.[11] Therefore, if quinoline based foldamers 4-to-66 units in length were to retain their conformation in a solvent, they would be expected to maintain a 2.0 nm diameter with a length ranging from 0.54 to 9.0 nm. However most standard DLS instruments are not able to detect objects whose dimensions are less than 2 nm, equivalent to a 15 quinoline-long foldamer. Moreover, the standard DLS instruments model macromolecular objects as spheres, which would lead to errors for large helical foldamers since such rigid symmetric top macromolecules might

require two diffusion coefficients, one to handle the rotation around the main axis and another for the tumbling around the secondary axis perpendicular to the main axis. Besides DLS, it was shown using Guinier plots obtained from X-ray scattering that the radius of gyration of an *m*-phenylene ethynylene (*m*PE) octadecamer in acetonitrile equaled 1.47 nm as expected.[24] While SAXS can probe the foldamer length scale at the nanometer level, the synchrotron high energy source implied that this study cannot be viewed as a routine experiment, and that the relatively high foldamer concentrations required (10^{-4}–10^{-3} M) could become an issue for less soluble foldamers.

By contrast, an earlier study on helical oligonucleotide duplexes and hairpins has established that time-resolved fluorescence anisotropy (TRFA) is ideally suited to study rigid symmetric top macromolecules with dimensions below 11 nm.[25] Furthermore, these TRFA experiments took advantage of the high sensitivity of fluorescence and were conducted at concentrations ranging between 10^{-5} and 10^{-4} M of macromolecular constructs, one order of magnitude lower than those conducted by SAXS. This study reports on the first example of the use of TRFA to probe the size and dynamics of a series of oligoquinoline foldamers in solution.

1.2 Quinoline-based foldamers labeled with oligo(phenylene vinylene)

Aromatic amide oligomers have many advantages as compared to other types of foldamers. These include the stability of the folded structure, predictability of the folding modes, propensity to crystallize, and relative ease of synthesis.[10,26] This thesis focuses on helical aromatic oligoamide foldamers synthesized from methyl-4-isobutoxy-8-nitroquinoline-2-carboxylate (Q_1), one of the most popular families of aromatic amide foldamers. A number of synthetic protocols have been established to prepare quinoline-based aromatic amide helical foldamers (Q_n).[10,26] The controlled addition of monomer Q_1 via amide coupling can result in the synthesis of Q_n foldamers with a sequence of up to 64 quinolines, that automatically adopt the helical conformation depicted in

Figure 1.1. Unfortunately, further elongation of these oligomers is prevented due to their poor solubility.

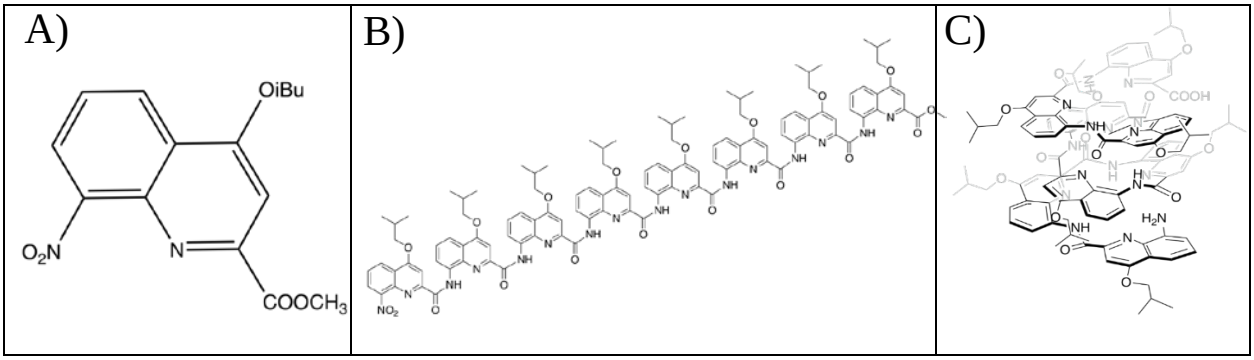

Figure 1.1. Chemical structure of A) methyl-4-isobutoxy-8-nitroquinoline-2-carboxylate (Q_1) and B) Q_8, and C) 3-D structure of helically folded octamer (Q_8).

The Q_8 oligomer can be used as a building block to generate more elaborate macromolecular constructs such as the photoactive triad shown in Figure 2, which is comprised of a central helical oligoamide foldamer bridge flanked by two chromophores.[7] The Q_8 foldamer provided a spacer of well-defined length to separate the oligo(*p*-phenylenevinylene) (OPV) electron acceptor at one end of the foldamer from the perylene *bis*-imide electron donor at the other end. The fact that the OPV did not seem to interact photochemically with the oligoquinoline backbone led to its selection for the TRFA study conducted in this project. A series of Q_n foldamers were synthesized with $n = 4 – 33$ and covalently labeled at their *N*-terminal with an OPV derivative bearing a carboxylic acid via a rigid amide bond to yield the series of OPV-Q_n constructs shown in Figure 1.2B. The angle between OPV and the main axis of the helical foldamer equaled 99.5 °, implying that OPV was almost perpendicular to the helix main axis.

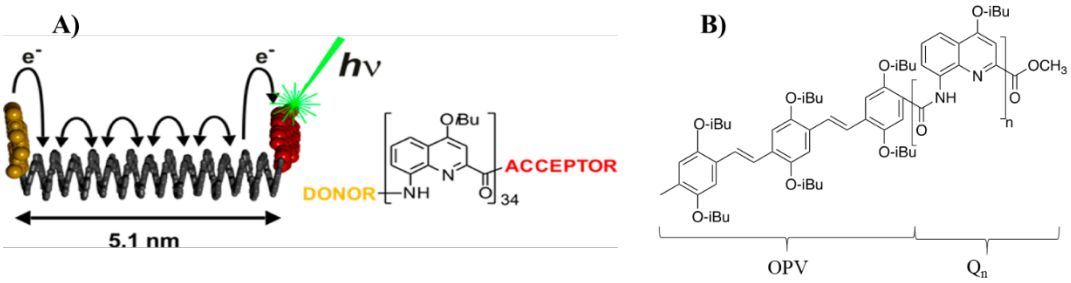

Figure 1.2. A) Structure of a photoactive triad comprised of a rigid foldamer bridge flanked by an electron donor OPV at one end and an electron donor perylene *bis*-amide at the other end. **B)** Chemical structure of OPV-Q_n.

1.3 Self-assembling foldamers via metal coordination

Besides the traditional synthetic protocols developed for the preparation of oligoquinoline foldamers, ligation of helical foldamers through their complexation by metal coordination represents an innovative method to generate longer strands. Furthermore, since complexation can take place at foldamer concentrations that are much lower than those required for foldamer synthesis, this method might circumvent the solubility issues plaguing the more traditional synthetic protocols. Oligoquinoline foldamers terminated with a carboxylic acid (Q_nA) offer a coordination site for metal cations such as Na^+, that enables the complexation of another Q_nA foldamer to form a two-strand metal complex (Q_nA-Na-Q_nA) as shown in Figure 1.3. The upfield shift of the signals in the ^1H NMR spectra, corresponding to the backbone amide protons of the Q_nA constructs, indicated the formation of a longer compound, while SCXRD showed that two Q_nA helical strands were coordinated to a Na^+ cation in an end-to-end fashion to form a continuous helix in the solid state. However, the conformation adopted by this complex in solution is still unknown.

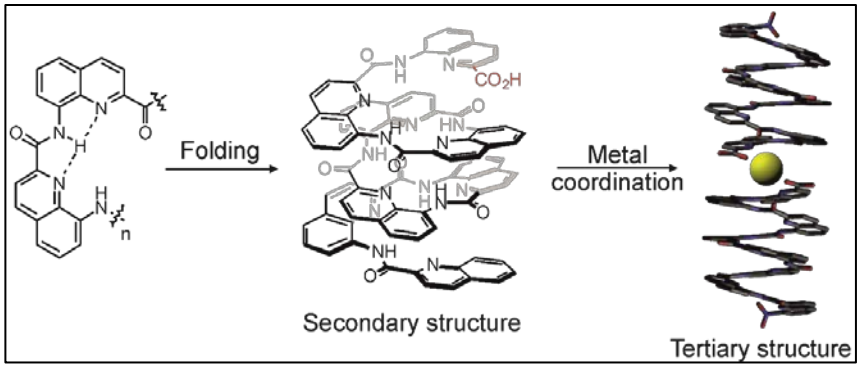

Figure 1.3. (Left and center) Scheme for the formation of a metal complex by metal coordination between two oligoquinoline foldamers terminated at one end with a carboxylic acid. (Right) Unpublished SCXRD structure obtained by Dr. Maurizot from the University of Bordeaux.

As depicted in Figure 1.3, the metal complexation of Q_nA foldamers with a single carboxylic acid per strand doubles the foldamer length through the formation of a Q_nA-Na-Q_nA complex. In contrast, the foldamer AQ_2PQ_2A bearing one acid group at both ends in Figure 1.4 could polymerize into much longer complexes. In fact, unpublished work from the University of Bordeaux showed that titration of a chloroform solution of a Q_8A-Na-Q_8A complex with increasing amounts of AQ_2PQ_2A can induce the formation of long insertion polymeric products of sequence Q_8A-Na-$(Q_2PQ_2$-Na$)_n$-Q_8A, where Q_8A acts as an end-capping agent.

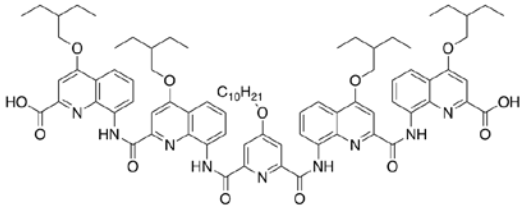

Figure 1.4. Chemical structure of AQ_2PQ_2A.

1.4 Time-resolved fluorescence anisotropy

Fluorescence anisotropy (r) measures the extent of depolarization of an excited chromophore after excitation by a photon obtained from a vertically polarized light source. Since the probability of exciting a photon depends on the squared cosine of the angle between the orientation of the excitation photons (i.e. vertical) and the absorption dipole moment of the chromophores randomly distributed in the solution, those chromophores whose absorption dipole moment is oriented vertically and parallel to the excitation polarization are most likely to become excited. This photoselection of the excited chromophores results in a difference between the photons emitted in the vertical and horizontal planes of detection. The anisotropy is determined by measuring the difference between the fluorescence intensity polarized in the vertical (I_{VV}) and horizontal (I_{VH}) directions following a vertically polarized excitation.[27] As time elapses and the excited fluorophore tumbles randomly in solution, the photoselection of the chromophores disappears, the I_{VV} and I_{VH} intensities become equal, and the anisotropy reaches zero. The characteristic time taken by the anisotropy to reach zero is described by the rotational time (ϕ) of the chromophore.[27] As shown in Equation 1.1, ϕ depends on the solvent viscosity (η), the hydrodynamic volume (V_h) of the chromophore, and the solution temperature. If the chromophore is rigidly bound to a macromolecule, tumbling of the chromophore reflects the tumbling of the macromolecule, and V_h represents the hydrodynamic volume of the macromolecule and the bonded chromophore. In turn, the hydrodynamic volume of a macromolecule can be determined from ϕ obtained from an anisotropy experiment, which is an interesting feature to probe the dimension of foldamers in solution.[27]

$$\phi = \frac{\eta V_h}{RT} \tag{1.1}$$

A time-resolved fluorescence anisotropy (TRFA) experiment begins by acquiring the fluorescence decay ($I_{VM}(t)$) of the chromophore at the magic angle (54.7 ^{o}) upon excitation with vertically polarized photons. Setting the emission polarizer at the magic angle ensures that the chromophore is not subject to any polarization effect. The $I_{VM}(t)$ decay is then fitted with an exponential according to Equation 1.2.

$$I_{VM}(t) = I_o \exp(-t/\tau_o) \tag{1.2}$$

In Equation 1.2, I_o is the initial fluorescence intensity at $t = 0$ and τ_o is the natural lifetime of the chromophore. In this thesis, the chromophore is OPV bound to the foldamer.

The vertically ($I_{VV}(t)$) and horizontally ($I_{VH}(t)$) polarized decays are then analyzed globally by fitting them to Equations 1.3 and 1.4, respectively.

$$I_{VV} = \frac{I_o}{3}\exp(-t/\tau_o)\times[1+2r(t)] \tag{1.3}$$

$$I_{VH}(t) = \frac{I_o}{3G}\exp(-t/\tau_o)\times[1-r(t)] \tag{1.4}$$

In Equations 1.3 and 1.4, G is used to normalize the $I_{VV}(t)$ and $I_{VH}(t)$ decays and is referred to as the G-factor, whereas $r(t)$ represents the TRFA. $r(t)$ can be approximated by a sum of exponentials as shown in Equation 1.5.

$$r(t) = r_o \sum_{i=1}^{n} a_i \times \exp(-t / \phi_i) \qquad (1.5)$$

In Equation 1.5, r_o is the anisotropy at time $t = 0$ and a_i and ϕ_i represent the i-th normalized pre-exponential factor and rotational time of the macromolecule, respectively. Fitting the polarized fluorescence decays $I_{VV}(t)$ and $I_{VH}(t)$ globally according to Equations 1.3 and 1.4 yields the rotational time ϕ. In turn, the rotational time provides information about the spherical or cylindrical geometry of the macromolecule, its dimensions, and its internal dynamics.

1.5 Outline

The primary goal of this project was to use TRFA to establish the relationship between the rotational time of quinoline-based foldamers and their chain length, and to apply this relationship to determine the dimensions of metal complexes formed between oligoamide foldamers in solution. The thesis describes how this goal was reached. It is divided in the following manner. The introduction chapter provides some background information on helical aromatic quinoline-based oligoamide foldamers (Q_n) and the principles of time-resolved fluorescence anisotropy (TRFA). The preparation of OPV labeled foldamer (OPV-Q_n) is described in Chapter 2. It closely follows the protocol published by the laboratory of Prof. Ivan Huc, formerly at the University of Bordeaux, France, and now at the University of Munich, Germany. A linear relationship was found in Chapter 3 between the rotational time of the OPV-Q_n foldamers and their number of units (NU), for foldamers with NU ranging between 4 and 33. The rotational times were obtained by global analysis of the polarized fluorescence decays of the OPV-Q_n foldamers using a monoexponential TRFA. The research described in Chapter 4 suggests that TRFA can be applied to measure the size

of foldamer complexes generated by the self-assembly of oligoquinoline foldamer acids. It also provides evidence that the metal coordination of foldamer acids can be used to form long and rigid helical structures equivalent to an OPV-Q_n foldamer made of 66 quinoline units. Chapter 5 summarizes the main results obtained so far for this project and makes suggestions for future work.

Chapter 2

Preparation of OPV-labeled oligoquinoline foldamers

2.1 Overview

The protocols applied in the synthesis of helical nanosized foldamers can be divided into two categories. The chromatography-free large-scale synthesis is used for shorter oligomers[26] such as the hexamer or octamer, whereas a segment doubling strategy is employed to prepare oligomers[10] longer than the hexadecamer.

The synthesis of aromatic helical foldamers starts with methyl-4-isobutoxy-8-nitroquinoline-2-carboxylate (Q_1), derived from dimethyl 2-(2-nitrophenylamino)-fumarate.[26] In the convergent scheme (Scheme 2.1), the dimer (Q_2) is obtained by coupling two monomers, the tetramer (Q_4) by coupling two dimers, and the hexamer (Q_6) is formed by coupling one tetramer and one dimer. Similarly, the octamer (Q_8) was prepared by adding the dimer to the hexamer.[26] Coupling of two oligomers requires that they be end-functionalized with either an amine, prepared by reduction of the N-terminal nitro group, or an acid chloride prepared by activating the terminal acid, obtained through the saponification of the C-terminal methyl ester with oxalyl chloride.[26] Since only the short acid-functionalized Q_2 foldamer was added to the amino terminal of other foldamers in Scheme 2.1, the formation of the unwanted anhydride by-product between two Q_2 acid groups could be avoided, since their smaller size prevented them from adopting a helical conformation, known to stabilize anhydrides obtained with longer strands. Excess reagent could simply be removed by recrystallization. Therefore, the procedure of adding short oligomers was found to result in high coupling yields and could be scaled up to achieve multigram syntheses for the preparation of relatively short oligoamide foldamers.[26] However this procedure failed to produce oligoquinolines much longer than the octamer, equivalent to a 1.1 nm-long foldamer.

One major challenge complicating the synthesis of longer nanosized foldamers is steric hindrance, affecting the terminal reactive groups, that results from the stable conformation of the foldamer. Furthermore, both reactants and products have poor solubility, and the reaction is moisture sensitive. As it turns out, these limitations can be overcome by using pure chemicals at high concentrations, and allowing the coupling reaction between long oligoquinolines to proceed for longer times.[10] The segment doubling strategy method developed by the Huc laboratory has allowed the gram-scale synthesis of nanosized helical aromatic foldamers, and the longest foldamer ever prepared and fully characterized was constituted of 64 quinoline units.[10] This iterative strategy is described in Scheme 2.1 for the preparation of a 16-mer by coupling an octamer amine with an octamer acid chloride, or for the preparation of a 32-mer by coupling a 16-mer amine with a 16-mer acid chloride, etc… Theoretically and based on Scheme 2.1, long foldamers should be easily achieved by doubling the segment length. In practice, however, problems arise due to the low reactivity of the amine end-group and the formation of anhydrides between two acid end groups. This complicates the purification of the products as compared to the synthesis of shorter foldamers.[2] In the protocol outlined in Scheme 2.1, chromatography was shown to be an effective method to separate the coupling products and unreacted starting materials, if some precautions were taken. For instance, the similar polarity of the product and the amine prevented their separation by column chromatography. Therefore, excess acid chloride was needed to consume all the amines before purification. Unfortunately, the anhydride was an unavoidable by-product, even if the system was maintained as anhydrous as possible. This impurity could be removed by refluxing the crude product in a pyridine/H_2O mixture, to hydrolyze the anhydride back into the acid. After this, the acid could be separated and recovered from the reaction mixture by column chromatography on silica gel.[2]

Earlier studies from the Duhamel Laboratory have established that oligo(phenylene vinylene) (OPV) would be a suitable dye to probe the hydrodynamic volume (V_h) of quinoline-based foldamers by fluorescence anisotropy. The OPV can be attached onto the foldamer by coupling the Q_n-amine foldamer with the OPV-acid chloride, prepared by chlorination of the OPV-acid with Ghosez reagent, in the presence of *N*,*N*-diisopropylethylamine DIPEA (Scheme 2.1).[7]

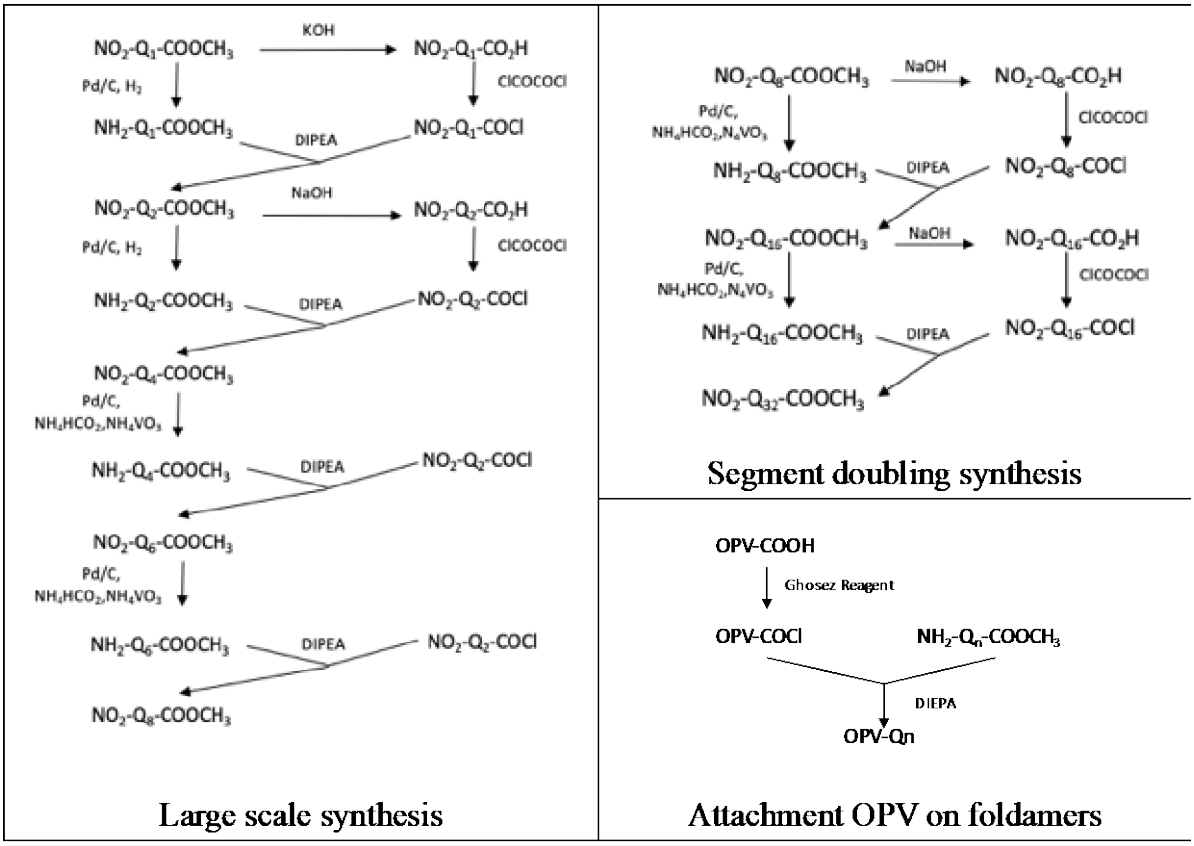

Scheme 2.1. Procedures used to synthesize foldamers and label them with OPV.

2.2 Materials

All the chemicals were bought from Sigma-Aldrich and were reagent grade, if not specifically mentioned. They include 2-methyl propanol (Alfa Aesar), 2-nitroaniline, anhydrous $MgSO_4$, CaH_2, Celite (VWR international), chloroform, chloroform-*d* (Euriso-top), dichloromethane, diisopropyl

azodicarboxylate, nitrogen, *N*,*N*-diisopropylethylamine (DIPEA), dimethyl acetylene dicarboxylate, diphenyl ether, ethyl acetate, hydrochloric acid (aqueous solution, minimum 37% (wt/wt)), hydrogen, isobutyl alcohol, methanol (MeOH), $NaHCO_3$, oxalyl chloride, Pd/C catalyst (10%) (Alfa Aesar), Q1and Q_7-NH_2 (H-lab), silica gel, sodium chloride, tetrahydrofuran (THF), and triphenylphosphine (Alfa Aesar). Distilled in glass toluene and HPLC-grade chloroform were purchased from Aldrich and used for the fluorescence anisotropy experiments. All the chemicals were used as received. The preparation of OPV-CO_2H, used to label the amino-terminal of the foldamers, has been described earlier.[6]

2.3 Equipment

Reactions were monitored by thin layer chromatography (TLC) on Merck silica gel 60-F254 plates and observed under UV light. Column chromatography purifications were carried out on Merck GEDURAN Si60 (40-63 µm). ESI mass spectra were obtained at the Mass Spectrometry Laboratory of the European Institute of Chemistry and Biology (UMS 3033 - IECB), Pessac, France, and at the Mass Spectrometry facility of the University of Waterloo, Canada. NMR spectra were recorded on an Avance II NMR spectrometer (Bruker Biospin) with a vertical 7.05 T narrow-bore/ultrashield magnet operating at 300 MHz for proton. The chemical shifts of the foldamers synthesized are reported in Appendix A in parts per million (ppm, δ) relatively to the ^1H residual signal of the deuterated chloroform (7.3 ppm). Preparative recycling Gel Permeation Chromatography (GPC) was performed on a JAI LC-9130G NEXT using two JAIGEL 20×600 mm columns (Japan Analytical Industry) with 0.5 % NEt_3 in chloroform (HPLC grade, ethanol-stabilized) as mobile phase, at a flow rate of 7 mL/min. After collection, the fractions were washed with a 5% NH_4Cl solution and twice with water.

2.4 Reagent and equipment setup

The dry DCM and THF were obtained by filtration through activated alumina using a dedicated purification system and needed to be used immediately after collection. The dry chloroform and anhydrous DIEPA were obtained by distillation over CaH_2. All the glass equipment and stir bars were dried in an oven, and the plastic syringes and needles obtained after opening their packaging were considered to be dry. When they were reused, they were cleaned with acetone and dried under vacuum.

2.5 Preparation of foldamers

The synthetic work to prepare the foldamers was entirely done at the Université de Bordeaux, France, in the Huc laboratory (H-Lab) under the supervision of Dr. Victor Maurizot.[1,2] Some of the foldamers used in this thesis were prepared in the H-Lab. The synthesis of the foldamers prepared by the author of this thesis is described hereafter.

2.5.1 Preparation of the dimer (Q_2)

First, the nitro group of Q_1 needed to be reduced to obtain the corresponding amine. Q_1 (6.8 g, 22.4 mmol) was dissolved in 150 mL of ethyl acetate in a reaction flask. The solution was flushed with nitrogen to purge the air before adding the Pd/C catalyst (10%, 680 mg) under nitrogen atmosphere. Then the flask was filled with hydrogen using a balloon. The reaction was conducted at room temperature and stirred under hydrogen atmosphere for 12 h to obtain Q_1-NH_2. The purity of the product was verified by ^{1}H NMR. The reaction mixture was filtered through Celite, washed with water and brine, dried over Na_2SO_4, filtered again and the solvent was removed under reduced pressure. Q_1-NH_2 was obtained in a 6.10 g (yield 99.5%) yield as a yellow solid.

The methyl ester of Q_1 needed to be deprotected to regenerate the acid functionality. Q_1 (7.2 g, 23.7 mmol) was dissolved in 290 mL of 1,4-dioxane and 30 mL of distilled water and KOH

powder (3.30 g, 58.9 mmol) was added to the solution. The reaction was stirred at room temperature and monitored by TLC until completion. The reaction was quenched with aqueous citric acid (5%, wt/wt) up to a pH around 5. Volatile components were removed under reduced pressure and the crude product was dissolved in DCM. The organic phase was washed with water and brine, dried over $MgSO_4$ and the solvent was evaporated to yield Q_1-CO_2H as a yellow solid (6.80 g, 23.4 mmol). Dry Q_1-CO_2H was dissolved in 45 mL anhydrous DCM and mixed with oxalyl chloride (10 mL, 117 mmol) under nitrogen atmosphere. After stirring for two hours at room temperature, the reaction was complete (as confirmed by NMR), and the solvent and remaining oxalyl chloride were removed under vacuum for 5 h to yield the Q_1-COCl product (6.9 g, 23.4 mmol, yield 98%).

The coupling of Q_1-NH_2 and Q_1-COCl was carried out in the presence of DIEPA. Q_1-NH_2 (6.10 g, 22.3 mmol) was added to 55 mL of anhydrous DCM under nitrogen, and dry DIEPA (21.3 mL) was added to the flask. Q_1-COCl (6.9 g) was dissolved in 50 mL DCM and transferred into the Q_1-NH_2 solution by syringe. After the reaction was stirred for 12 h, the Q_2 dimer was obtained. The workup was finished by precipitating the reaction mixture with MeOH and washing the product with water. The purity of Q_2 (7.5 g, yield 61%) was confirmed by NMR.

2.5.2 Preparation of the tetramer (Q_4)

The reduction of Q_2 (2.9 g, 5.31 mmol) proceeded in a manner similar to that of Q_1, except that it was conducted with 340 mL ethyl acetate and 290 mg Pd/C catalyst at 50 ^oC under a nitrogen atmosphere. The reduction yielded 2.70 g of Q_2-NH_2 (yield 98%), which could be used for the coupling reactions.

The saponification of Q_2 (8.90 g, 16.3 mmol) was conducted in a manner similar to Q_1-CO_2H, except that 270 mL of THF and 90 mL methanol were used to dissolve the starting material,

and NaOH (2.00 g, 50 mmol) was employed. After workup, 8.60 g (yield 98%) of Q_2-CO_2H was recovered. A fraction of the recovered Q_2-CO_2H (5.64 mmol) was dissolved in 45 mL of dry DCM, to which 2.4 mL oxalyl chloride (28.0 mmol) was added under nitrogen atmosphere to activate the acid. The same procedure as for Q_1-COCl was applied for the workup of Q_2-COCl.

Similarly, the coupling of Q_2-NH_2 (1.7 g, 3.29 mmol) and Q_2-COCl (1.8 g) was conducted in the same manner as before. The amounts of DIEPA, DCM for the Q_2-NH_2 amine, and DCM for the acid chloride were 5, 10, and 40 mL, respectively. The product Q_4 was recovered with 3.2 g yield (yield 91%) .

2.5.3 Preparation of the hexamer (Q_6)

The preparation of the hexamer started with the reduction of Q_4 (3.1 g, 3 mmol) dissolved in 120 mL ethyl acetate and 30 mL ethanol. The solution was placed under nitrogen atmosphere before adding 300 mg of Pd/C (10%) catalyst and a catalytic amount of ammonium metavanadate at room temperature. An aqueous solution of ammonium formate (45-50 equiv) was slowly added to the reaction mixture in 3 to 5 portions at 95 ^oC. The reaction was allowed to react for 12 h and was monitored by NMR until it was complete. After workup, 2.95 g, equivalent to 2.94 mmol of Q_4-NH_2, was obtained as a yellow solid (yield 98%).

The reduction of Q_4 was followed by the activation of Q_2-CO_2H (1.68 g, 3.18 mmol) with 1.6 mmol oxalyl chloride. Q_6 was prepared by coupling Q_2-COCl with Q_4-NH_2 in the presence of 3 mL DIEPA. After workup, 3.36 g (2.24 mmol) of Q_6 was obtained (yield 76%).

2.5.4 Preparation of the octamer (Q_8)

The reduction of Q_6 (3.36 g, 2.24 mmol) was carried out in a mixture of 106 mL ethyl acetate and 26 mL EtOH with 0.336 g of Pd/C catalyst, 0.17 g ammonium metavanadate, and an aqueous solution of NH_4HCO_2 (40 to 50 equivalents relatively to Q_6). The workup procedure was the same

as for Q_4-NH_2, and 2.9 g (2 mmol) of Q_6-NH_2 was obtained (yield 89%). Q_8 was obtained by coupling Q_6-NH_2 and Q_2-COCl in equimolar amounts (2.1 mmol each) in the presence of DIEPA (1.93 mL). The workup yielded Q_8 (3 g, 1.5 mmol, yield 75%).

2.5.5 Preparation of the 16-mer (Q_{16})

To 25 mL of a 4:1 mixture of EtOAc:EtOH was added Q_8 (1.1 g, 0.55 mmol), Pd/C catalyst (10%, 0.1 g), and ammonium metavanadate (catalytic amount) at room temperature. The mixture was heated to 95 ^oC and 1.42 g of 1.7 mM ammonium formate in water was added in 5 portions. The reaction was stirred overnight at 95 ^oC. After applying the same workup as in the other reductions, Q_8-NH_2 (1.06 g, 0.5 mmol, and yield 90%) was recovered as a yellow powder (yield 90%).

Q_8 (2 g, 1 mmol) was dissolved in 70 mL THF and 7.7 mL MeOH before ground NaOH powder (0.8 g, 130 mL) was added. The mixture was stirred at room temperature for around 0.5 h and monitored by TLC until the reaction was complete. After workup, the reaction yielded 1.65 g (0.8 mmol) of Q_8-COOH (yield 80%). Dry Q_8-COOH (1.48 g, 0.75 mmol) was dissolved in 5.77 mL of $CHCl_3$ to which was added 0.64 mL of oxalyl chloride. The mixture was stirred for 2 h. The liquid was removed under reduced pressure to yield Q_8-COCl (1.49 g, yield 100%).

To a solution of Q_8-NH_2 (1.06 g, 0.5 mol) and DIEPA (0.25 mL) in $CHCl_3$ (3.38 mL) was added a Q_8-COCl (1.49 g, 0.75 mmol) solution in $CHCl_3$ (5 mL). The mixture was stirred overnight at room temperature and monitored by NMR until the peak for the amine completely disappeared. The solution was evaporated under reduced pressure to remove the solvent and the product was refluxed in a mixture of pyridine/H_2O (10 mL/2 mL) for 12 h to hydrolyze the anhydride by-product. Then pyridine and H_2O were removed by azeotropic distillation with toluene, and the residue was purified by silica gel chromatography using a DCM/EtOAc mixture as eluent to yield Q_{16} (1 g, 250 μmol, yield 50%).

2.5.6 Preparation of the 24-mer (Q_{24})

The reduction of Q_{16} was conducted in a manner similar to that applied to reduce Q_8. After conducting the reaction with Q_{16} (100 mg, 26 μmol), EtOAc (4 mL), EtOH (1 mL), ammonium metavanadate (2 mg), Pd/C catalyst (10 mg), ammonium formate (95 mg), and H_2O (0.25 mL), 96 mg (25 μmol) of Q_{16}-NH_2 was obtained (yield 96%). The activation of Q_8-CO_2H (250 mg, 127 μmol) in 1.39 mL $CHCl_3$ with 0.073 mL of oxalyl chloride yielded the activated Q_8-COCl (127 μmol, yield 100%). Coupling Q_{16}-NH_2 (26 μmol) with Q_8-COCl (127 μmol) overnight in the presence of 0.015 mmol DIEPA in 0.4 mL $CHCl_3$ yielded Q_{24}. The work up was the same as for Q_{16} resulting in 100 mg, 17 μmol of pure Q_{24} (yield 70%).

2.5.7 Preparation of the 32-mer (Q_{32})

The saponification of Q_{16} was conducted in the same manner as for Q_8. Q_{16} (700 mg, 177 μmol) was dissolved in 25 mL THF and 3 mL MeOH. NaOH (140 mg) was added to the mixture to yield Q_{16}-CO_2H (664 mg, 170 μmol, yield 76%). The activation of Q_{16}-CO_2H was carried out in 3.65 mL $CHCl_3$ with 0.073 mL oxalyl chloride (170 μmol, yield 100%).

The coupling of Q_{16}-NH_2 (237 mg, 70 μmol) and Q_{16}-COCl (170 μmol) was achieved with 0.04 mL of DIEPA in 5 mL $CHCl_3$. The anhydride by-product was removed by refluxing in a pyridine/H_2O (5 mL/0.5 mL) mixture before using silica gel chromatography to isolate the product. In the end, 130 mg (17.9 μmol) of Q_{32} was recovered (yield 26%).

2.5.8 Preparation of OPV-Q_7

Q_7-NH_2 (20 mg, 11.5 μmol) and OPV-COCl (23 μmol), which had both been synthesized in the H-Lab,[6] were reacted in the presence of DIEPA (3.7 μL). OPV-COCl was produced by the

activation OPV-CO_2H (17.8 mg, 23 μmol) with 35 μmol of Ghosez reagent (1-chloro-N, N, 2-trimethyl-1-propenylamine) in $CHCl_3$. Purification was completed by GPC.

2.5.9 Preparation of OPV-Q_{24}

The reduction of Q_{24} was carried out in the same manner as for the other foldamers. Q_{24} (50 mg, 8.5 μmol) was dissolved in a mixture of 4 mL EtOAc and 1 mL EtOH in the presence of 0.8 mg ammonium metavanadate, 5 mg Pd/C (10%) catalyst, 32 mg ammonium formate, and 0.085 mL H_2O. The reduction was carried out under nitrogen atmosphere. The mass of Q_{24}-NH_2 recovered after workup equaled 30 mg. Q_{24}-NH_2 (30 mg, 5 μmol) was coupled with OPV-COCl (7.5 mg, 10 μmol) in the presence of DIEPA (3.7 μL). The final product was purified by GPC.

2.5.10 Preparation of OPV-Q_8A

Q_8-NH_2 (150 mg, 77 μmol) was coupled with OPV-COCl (1.19 g, 1.5 mmol) in chloroform after stirring overnight in the presence of DIEPA (0.25 mL). The final product was purified by GPC to yield 150 mg OPV-Q_8. Dry OPV-Q_8 (150 mg, 55 μmol) was dissolved in 38 mL THF and 0.5 mL MeOH before 60 mg ground NaOH powder was added. The mixture was stirred at room temperature for 30 min and monitored by TLC until the reaction was complete. This reaction yielded 123 mg, 45μmol OPV-Q_8A (yield 58%) .

2.5 Summary

The work reported in this thesis describes the behavior in solution of a series of oligoquinoline (Q_n) foldamers with a number of quinoline units ranging from 1 to 33, terminated by either ester (Q_n) or carboxylic acid (Q_nA) groups. The Q_n or Q_nA oligomers were linked to OPV-CO_2H to form the OPV-labeled Q_n esters (OPV-Q_n) with *n* equal to 4, 7, 9, 17, 24, and 33 and the OPV-labeled acids (OPV-Q_nA) with *n* equal to 4, 8, 17, and 33. Their purity was established by ^{1}H NMR and MS. The chemical structure of the foldamers used in this study is provided in Table 2.1. Beside

the samples synthesized in Bordeaux by the author, OPV-Q_4, OPV-Q_4A, OPV-Q_9, OPV-Q_{17}A, OPV-Q_{17}, OPVOPV-Q_{33}A, OPV-Q_{33}, and AQ_2PQ_2A (with hexyl or isobutyl side chain) were also prepared in the H-Lab and were used as received.

Table 2.1. Chemical structure of the samples used in this study.

Chemical structure	Samples	Number of Units
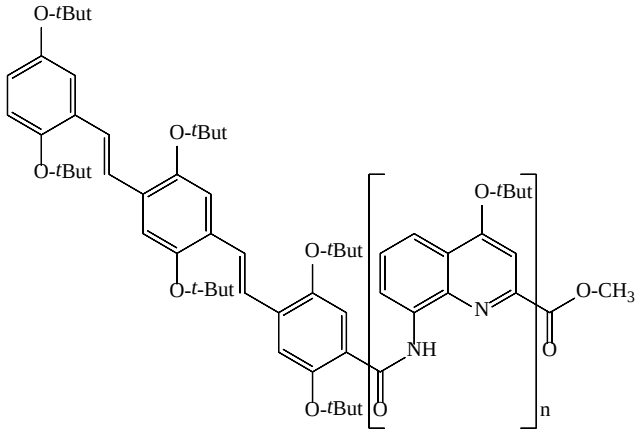	OPV-Q_4	4
	OPV-Q_7	7
	OPV-Q_9	9
	OPV-Q_{17}	17
	OPV-Q_{24}	24
	OPV-Q_{33}	33
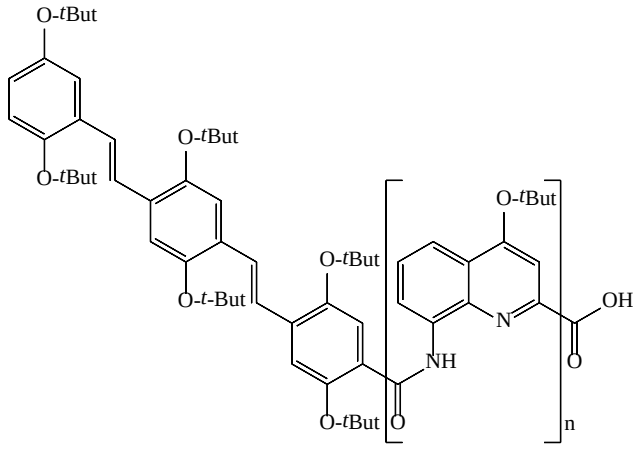	OPV-Q_4A	4
	OPV-Q_8A	8
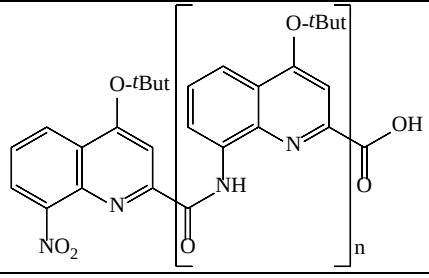	Q_8A	8
	Q_{16}A	16

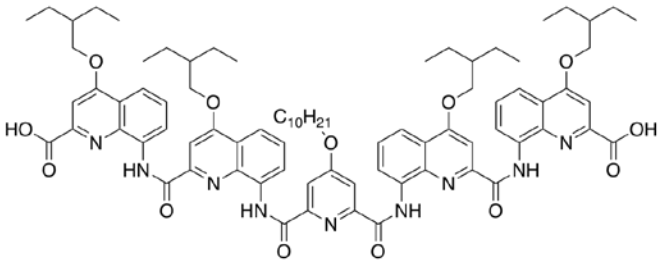	AQ_2PQ_2A	

Chapter 3

Application of TRFA to probe OPV-Q_n

3.1 Introduction

The preparation of quinoline-based foldamers with up to 64 units has been published by the H-Lab. The conformation and dimension of the foldamers were investigated by SCXRD analysis. They were found to fold as helices in the solid state, with a 0.136 nm raise per quinoline unit. The relatively small size of the foldamers complicates their characterization in solution, as discussed in the Introduction. Therefore, TRFA was applied to probe the size and conformation of the foldamers in solution, as has been done earlier to study a series of well-defined DNA duplexes in solution.[25]

In this chapter, a series of quinoline-based foldamers (Q_n with n =1 – 33) was prepared and they were labeled with an oligo(phenylene vinylene) (OPV) fluorophore. Time-resolved fluorescence anisotropy (TRFA) experiments were conducted by acquiring the fluorescence decays for OPV-Q_n solutions in chloroform with a vertically polarized excitation, and an emission that was polarized either vertically or horizontally to yield the fluorescence decays $I_{VV}(t)$ and $I_{VH}(t)$, respectively. The rotational time (ϕ) of the OPV-Q_n molecules was retrieved from the global analysis of the $I_{VV}(t)$ and $I_{VH}(t)$ fluorescence decays. This chapter explains how the relationship between the rotational time and the oligoquinoline chain length was established to probe the helical conformation of foldamers in solution. Furthermore, the use of the diffusion coefficients ($D_{//}$) and ($D_{\perp}$), describing the rotation of the foldamers around and perpendicularly to the main helix axis, respectively, was also discussed to rationalize the anisotropy results.

3.2 Experimental

3.2.1 Materials

Chloroform (HPLC grade) was used as received for all the fluorescence experiments. The chemical structure of the OPV-Q_n and Q_nA oligomers used in this study is presented in Figure 3.1.

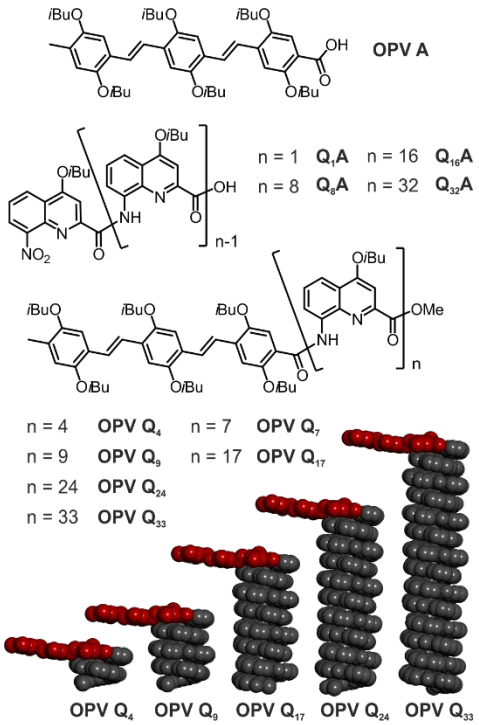

Figure 3.1. Chemical formula of the oligoquinoline foldamers and energy-minimized molecular models of the oligomers, with the OPV unit in red to illustrate its orientation perpendicular to the helical axis. *iso*-Butoxy side chains and protons are omitted for clarity.

3.2.2 Instrumentation

Absorption measurements: The absorption spectra were acquired on a Cary 100 UV-Vis spectrophotometer with quartz cells having a 1 cm path length.

Steady-State Fluorescence (SSF): Fluorescence spectra for OPV-Q_n solutions in chloroform were acquired with a Photon Technology International LS-100 steady-state fluorometer using the right-

angle geometry. The OPV-Q_n samples were excited at 408 nm and the fluorescence spectra were acquired from 420 to 700 nm.

Time-resolved fluorescence anisotropy (TRFA): TRFA measurements were conducted with a HORIBA Ultima Ultrafast Fluorescence Lifetime Spectrofluorometer equipped with a delta diode laser having a maximum emission intensity at 479 nm, to selectively excite the OPV fragment of the OPV-Q_n foldamers (see Figure 3.2). The fluorescence decays were acquired with a Picosecond Photon Detection (PPD) Module 650, using a 495 nm cut-off filter to minimize scattered light from reaching the detector. The fluorescence intensity was controlled with neutral density filters and the width of the emission monochromator slits was set at 12 nm. The instrument response function was collected by monitoring the light reflected by a metal mirror at $\lambda_{em} = \lambda_{ex} = 479$ nm without the 495 nm cut-off filter. All the fluorescence decays were measured with a time-per-channel (TPC) of 12.8 ps/ch over 4,096 channels, except for the OPVA molecule whose shorter rotational time of 270 ps required a TPC of 1.37 ps/ch for more accurate analysis. For each OPV-Q_n sample, a small amount of OPV-Q_n was dissolved and diluted in chloroform to obtain an absorbance at 479 nm of 0.09 OD, corresponding to an OPV-Q_n concentration of 1.4×10^{-5} M assuming a molar extinction coefficient at 479 nm of 6,250 $M^{-1}.cm^{-1}$ for OPV bound to the foldamers (see Results and Discussion section). The fluorescence decays were acquired using excitation light that was vertically polarized (V) and with the emission polarizer oriented at the magic angle ($I_{VM}(t)$), parallel ($I_{VV}(t)$), and perpendicular ($I_{VH}(t)$) to the vertically polarized excitation light. The analysis for a TRFA experiment began by fitting with a single exponential the fluorescence decay for the dye acquired with the excitation and emission polarizers set in the vertical and magic angle (54.7 ^{o}) orientations, respectively. The magic angle orientation used for the $I_{VM}(t)$ decay eliminates polarization effects.[27] All the fluorescence decays were acquired with

10,000 and 20,000 counts at the decay maximum. The fit of the $I_{VM}(t)$ decays yielded a natural lifetime (τ_o) of 1.6 ns for the OPV. The vertically ($I_{VV}(t)$) and horizontally ($I_{VH}(t)$) polarized fluorescence decays were fitted to Equations 3.1 and 3.2, respectively, which were presented as Equations 1.3 and 1.4 in the first chapter.

$$I_{VV} = \frac{I_o}{3}\exp(-t/\tau_o)\times[1+2r(t)] \qquad (3.1)$$

$$I_{VH}(t) = \frac{I_o}{3G}\exp(-t/\tau_o)\times[1-r(t)] \qquad (3.2)$$

In Equation 3.1 and 3.2, G is the G-factor for TRFA measurements and $r(t)$ represents the TRFA.[27] Contrary to classic experimental set ups for TRFA measurements for which the intensity of the excitation source must be carefully monitored to determine the G-factor by flipping the emission polariser at set times between the vertical and horizontal positions, Equations 3.1 and 3.2 make it clear that the G-factor is only a scaling factor which needs to be optimized in the global analysis of the fluorescence decays. The advantage of this approach is that it does away with the tedious and time-consuming alternation of polarizer orientations, so that both decays can be acquired with the same number of counts at the decay maximum to maximize the signal-to-noise ratio, which is inherently impossible to achieve with the standard procedure. Additional experimental details about this procedure can be found in Appendix B. All the TRFA could be approximated by a single exponential, as shown in Equation 3.3. The program written in house to fit the $I_{VV}(t)$ and $I_{VH}(t)$ decays globally was aniso01c.

$$r(t) = r_o \times e^{-t/\phi} \qquad (3.3)$$

The I_{VV}(t) and I_{VH}(t) decays acquired with 20,000 counts at the decay maximum were also fitted with a triexponential TRFA, and the program used for this analysis was aniso02n-3. Global analysis of the polarized fluorescence decays $I_{VV}(t)$ and $I_{VH}(t)$ according to Equations 3.1 and 3.2 yielded good fits, with a χ^2 parameter smaller than 1.3 and the residuals and autocorrelation of the residuals evenly distributed around zero. All the parameters retrieved from the analysis of the fluorescence decays are listed in Appendix D. Each TRFA measurement was conducted in triplicate to assess the error in the rotational times.

The rotational time of the OPV-labeled foldamers was then related to the hydrodynamic volume of the macromolecules according to Equation 1.1. It must be stated that, strictly speaking, Equation 1.1 should only be used for spherical objects, which the OPV-labeled foldamers are not. Nevertheless, it was found to satisfyingly describe these constructs over the range of foldamer lengths studied in this chapter, and it was used as an empirical expression to describe the rotational time of the foldamers.

Approximating the shape of the foldamer to a cylinder implied that V_h would be a function of the squared hydrodynamic radius (R_h^2) of the cylinder, which is constant, the height of the foldamers, which is related to the number of units (*NU*) in the foldamer, the helical rise per quinoline residue (Δh), and the volume (V_o) of the OPV label, as shown in Equation 3.4. Consequently, ϕ was expected to increase linearly with increasing number of quinoline units (*NU*) when the temperature and viscosity of the solution remained constant.

$$\phi = \frac{\eta}{k_B T} \times (V_o + \Delta h \times NU) \qquad (3.4)$$

Since Δh is known to equal 0.136 nm based on a pitch of 0.34 nm for an oliquinoline helix containing 2.5 quinolines per helical turn, Equation 3.4 implies that a plot of ϕ-versus-NU should yield a straight line if the OPV-labeled foldamers adopted a rigid helical conformation in solution.

3.3 Results and Discussion

This study aimed to apply TRFA to characterize the size of a series of oligoquinolines in solution. The chromophore OPV was rigidly attached onto the foldamers via an amide bond, so that its tumbling in solution probed by TRFA closely reflected that of the foldamers. Since the absorbance spectrum for the oligoquinoline backbone overlapped with that for the OPV, the excitation and emission wavelengths employed in the TRFA measurements needed to be carefully selected.

3.3.1 Quantum yield of OPV

The OPV-Q_n samples were excited at 408 nm and the fluorescence spectra were acquired from 420 to 700 nm. The quantum yield (Φ_{OPV}) of OPV-Q_8A in chloroform was calculated by applying Equation 3.5,

$$\Phi_{OPV} = \Phi_{PBA} \times \frac{I_F(OPV)}{I_F(PBA)} \times \frac{Abs(PBA)}{Abs(OPV)} \times \frac{n_{Chl}^2}{n_{CX}^2} \qquad (3.5)$$

where 9,10-bis(phenyl-ethynyl) anthracene (BPA) was used as a fluorescence standard (Φ_{PBA}=1 in cyclohexane),[28] I_F(OPV) and I_F(PBA) are the fluorescence intensity obtained from the integration from 440 to 680 nm of the fluorescence spectra for solutions of OPV in chloroform and PBA in cyclohexane, having absorptions *Abs*(OPV) and *Abs*(PBA) at 430 nm of 0.047 and

0.049, respectively. The refractive indices n_{Chl} and n_{CX} of chloroform and cyclohexane were taken as 1.446 and 1.426, respectively.[29] Φ_{OPV} for the OPV-Q_8A foldamer in chloroform was determined to equal 0.62 ± 0.04.

3.3.2 Absorption and fluorescence spectra

The spectra for the molar extinction coefficient (MEC) of Q_8A (dashline) and OPVA (solid line) and the fluorescence of OPVA are shown in Figure 3.2. The absorption and fluorescence spectra of oligoquinoline and OPVA match those reported in the literature.[7] Although the molar extinction coefficient of OPVA passes through a maximum at 430 nm, the oligoquinoline backbone exhibits residual absorption at this wavelength. To avoid any complications, all the fluorescence decays were acquired with a 479 nm excitation wavelength and the fluorescence was collected at 510 nm. This wavelength selection ensured that the excitation photons would solely target the OPV fluorophore while yielding a strong enough fluorescence signal, regardless of the quantity of oligoquinoline foldamer present in the solution.

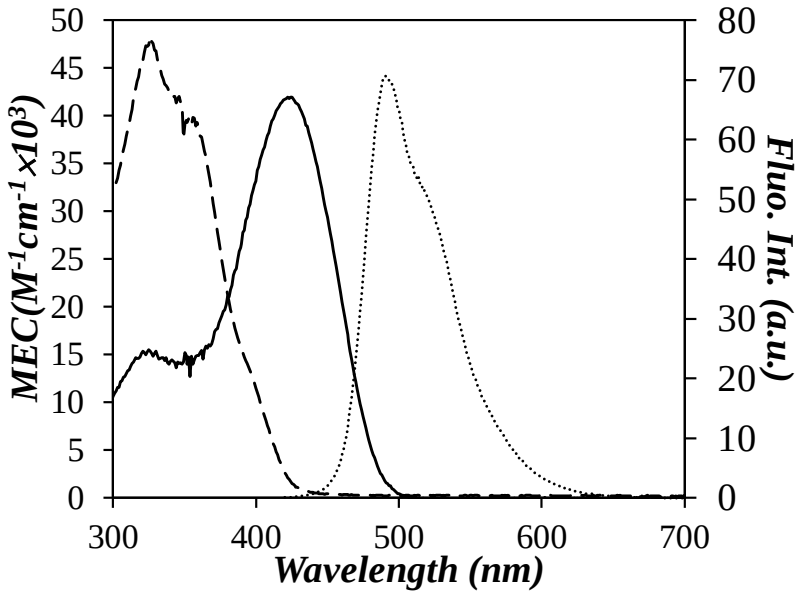

Figure 3.2. Spectra for the molar extinction coefficient of Q_8A (- -) and OPVA (—), and fluorescence of OPVA (···) in chloroform. Conditions for the fluorescence spectrum: [OPVA] = 2.6×10^{-6} mol.L^{-1} and λ_{ex} = 408 nm.

Based on their chemical composition shown in Figure 3.1, the absorption of the OPV-Q_n foldamers should show a linear increase in the relative absorption of the oligoquinoline backbone with respect to that of OPV when plotted as a function of the number of units (*NU*) of the foldamers. This is indeed observed in Figure 3.3A for the OPV-Q_n foldamers, where the absorption spectra were normalized to a value of unity at 450 nm where only OPVA absorbs (see Figure 3.2). The relative absorption of the oligoquinoline backbone was found to increase with increasing foldamer length. This trend was better illustrated by plotting the ratio of the absorbance at 326 nm over that at 450 nm, namely the *Abs*(326nm)/*Abs*(450nm) ratio as a function of the number of quinoline units in Figure 3.3B. The linear trend obtained in Figure 3.3B is predicted by Equation 3.6, where ε_{OPV}(326 nm), ε_{OPV}(326 nm), and ε_{OPV}(450 nm) are the molar extinction coefficient (MEC) of the OPV moiety at 326 nm, one quinoline moiety at 326 nm, and the OPV moiety at 450 nm,

respectively. The MEC of one quinoline moiety was determined experimentally by plotting in Figure 3.3C the MEC at 326 nm (ε_{Q_nA}(326 nm)) of the Q_1A, Q_8A, Q_{16}A, and Q_{32}A foldamers, which were available in larger quantities, as a function of the number of quinoline units. A linear relationship was obtained with a slope of 5,600 ± 130 $M^{-1}.cm^{-1}$, a value consistent with ε_Q (326 nm) of Q_1 found to equal 5,840 (±100) $M^{-1}.cm^{-1}$.

$$\frac{Abs(326\,nm)}{Abs(450\,nm)} = \frac{\varepsilon_{OPV}(326\,nm)}{\varepsilon_{OPV}(450\,nm)} + NU \times \frac{\varepsilon_{Q}(326\,nm)}{\varepsilon_{OPV}(450\,nm)} \tag{3.6}$$

The intercept of the line in Figure 3.3B was found to equal 0.41 ($\pm$ 0.09) which is comparable within experimental error with the ε_{OPV}(326 nm)/ε_{OPV}(450 nm) ratio used in Equation 3.6, found to equal 0.52 for OPVA. The slope (*m*) of the straight line in Figure 3.3B equaled 0.173 ($\pm$0.005). According to Equation 3.6, dividing ε_Q(326 nm) by *m* should yield ε_{OPV}(450 nm). The ratio ε_Q(326 nm)/*m* equaled 32,400 (±750) $M^{-1}.cm^{-1}$, which is consistent with the MEC value of 29,300 $M^{-1}.cm^{-1}$ at 450 nm for OPVA. However, since the MEC value of 32,400 (±750) $M^{-1}.cm^{-1}$ was obtained for the OPV bound to the foldamers, it is this value and not that of 29,300 $M^{-1}.cm^{-1}$ found for OPVA that was used to calculate the concentration of OPV-labeled foldamers by UV-Vis absorption.

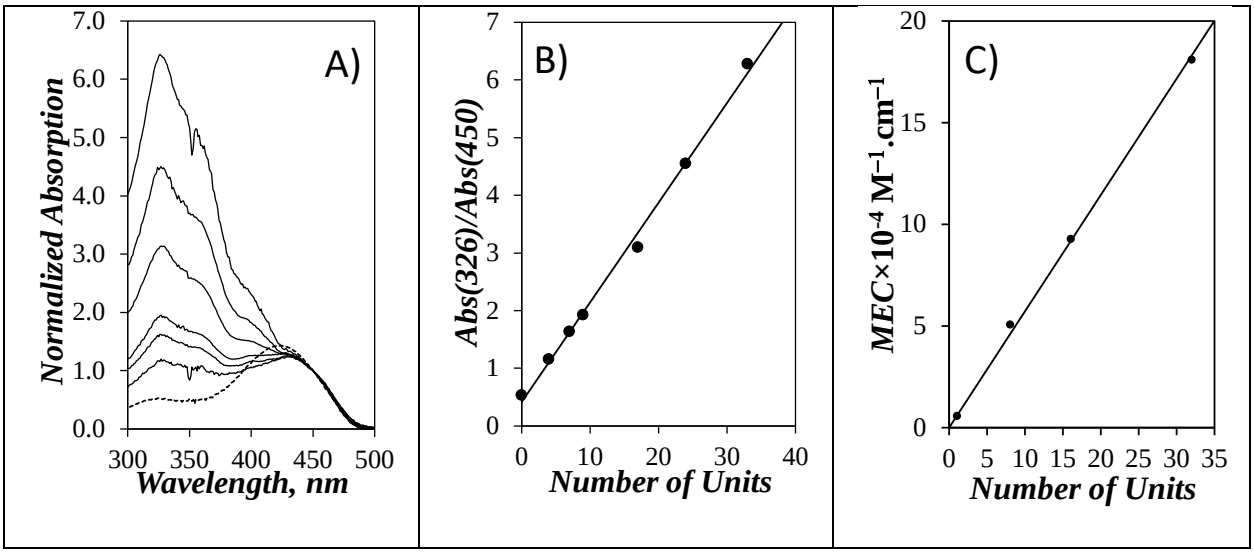

Figure 3.3. A) Absorption spectra normalized at 450 nm. Bottom to top: OPVA (dashed line), and OPV-Q_4, OPV-Q_7, OPV-Q_9, OPV-Q_{17}, OPV-Q_{24} and OPV-Q_{33}. Plots of B) the Abs(326 nm)/Abs(450 nm) ratio and C) the molar extinction coefficient at 326 nm for the Q_1A, Q_8A, Q_{16}A, and Q_{32}A foldamers as a function of the number of quinoline units.

3.3.3 Time-resolved fluorescence anisotropy

For each solution of 1.4×10^{-5} M OPV-labeled foldamer in chloroform, a set of three fluorescence decays were acquired with the excitation light polarized vertically and the emission polarizer oriented at the magic angle, vertically, and horizontally to obtain the $I_{VM}(t)$, $I_{VV}(t)$, and $I_{VH}(t)$ fluorescence decays, respectively. Figure 3.4 presents the three decays for OPV-Q_{33} as an example. The fits were good, yielding low χ^2 values (< 1.3), and randomly distributed residuals and autocorrelation of the residuals.

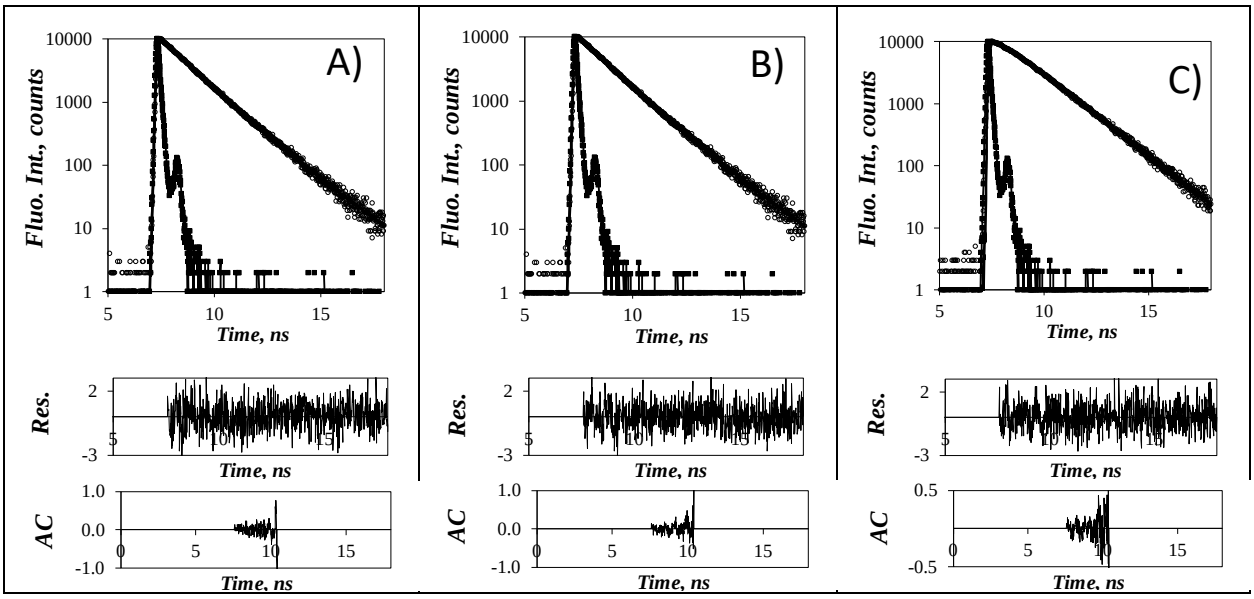

Figure 3.4. Global analysis of the A) $I_{VM}(t)$, B) $I_{VV}(t)$, and C) $I_{VH}(t)$ fluorescence decays of OPV-Q_{33} with Equations 1-2. λ_{ex} = 479 nm, λ_{em} = 510 nm, χ^2 = 1.16.

Global analysis of the $I_{VV}(t)$ and $I_{VH}(t)$ fluorescence decays according to Equations 3.1 and 3.2, respectively, yielded the rotational time (ϕ) of the OPV-labeled foldamers. A plot of ϕ as a function of the number of units (*NU*) in the foldamer is shown in Figure 3.5. Within experimental error, all the ϕ values were clustered around a straight line as predicted by Equation 3.4. The intercept ϕ_o of the line with the y-axis equaled 0.32 (± 0.03) ns, which matches fairly closely the rotational time of 0.27 (± 0.02) ns for OPVA. Consequently, the trend shown in Figure 3.5 indicates that the hydrodynamic volume of an OPV-labeled foldamer increases linearly with the number of quinoline residues. This conclusion agrees with the notion that the oligoquinoline foldamers adopt a helical conformation in chloroform, whereby the addition of a single quinoline residue increases the volume of the foldamer by a set increment. A similar behavior has also been reported earlier, when monitoring the rotational time of a series of helical DNA duplexes as a function of the number of base pairs of the oligonucleotides.[25]

The line in Figure 3.5 has a slope of 0.057 (± 0.001) ns. Based on the curvature of the helix, an oligoquinoline helix has 2.5 quinoline units per turn, and a pitch of 0.34 nm, and each quinoline unit contributes 0.136 nm to the helix. According to these parameters, Equation 3.4 suggests that the hydrodynamic radius of a Q_n foldamer equals 1.01 (± 0.01) nm. The radius obtained by TRFA measurements is consistent with the 1.0 nm radius of Q_n foldamers determined by SCXRD.[8] Based on Equation 3.4, the straight line obtained in Figure 3.5A implies that the volume of a Q_n foldamer is proportional to the number of its constituting quinoline units (*NU*). This behavior is very different from that expected for a flexible chain adopting a random coil conformation. In such a case the volume, and thus the rotational time of the macromolecule should increase as $NU^{3\nu}$, where ν is the Flory exponent equal to 0.5 or 0.6 in a θ– or a good solvent, respectively. Regardless of whether ν equals 0.5 or 0.6, a dependency for ϕ as $NU^{3\nu}$ would result in a much steeper increase in rotational time than that shown in Figure 3.5B. Consequently, the linear increase observed for ϕ in Figure 3.5 rules out the possibility that the Q_n foldamers adopt a random coil conformation in chloroform.

Since the molar concentration of the foldamers was fixed to equal 1.4×10^{-5} M in the experiments conducted to obtain the results shown in Figure 3.5, the mass concentration of foldamer increased with increasing foldamer length. To ensure that the results presented in Figure 3.5 were not due to the aggregation of OPV-Q_n foldamers, that would increase with increasing foldamer length and poorer solubility, the OPV-Q_{33} solution in chloroform was diluted 10-fold and the rotational time of the foldamer was monitored as a function of concentration. As can be seen in Appendix C, the rotational time of the OPV-Q_{33} foldamer remained constant with the foldamer concentration, demonstrating the absence of aggregation for the solutions investigated.

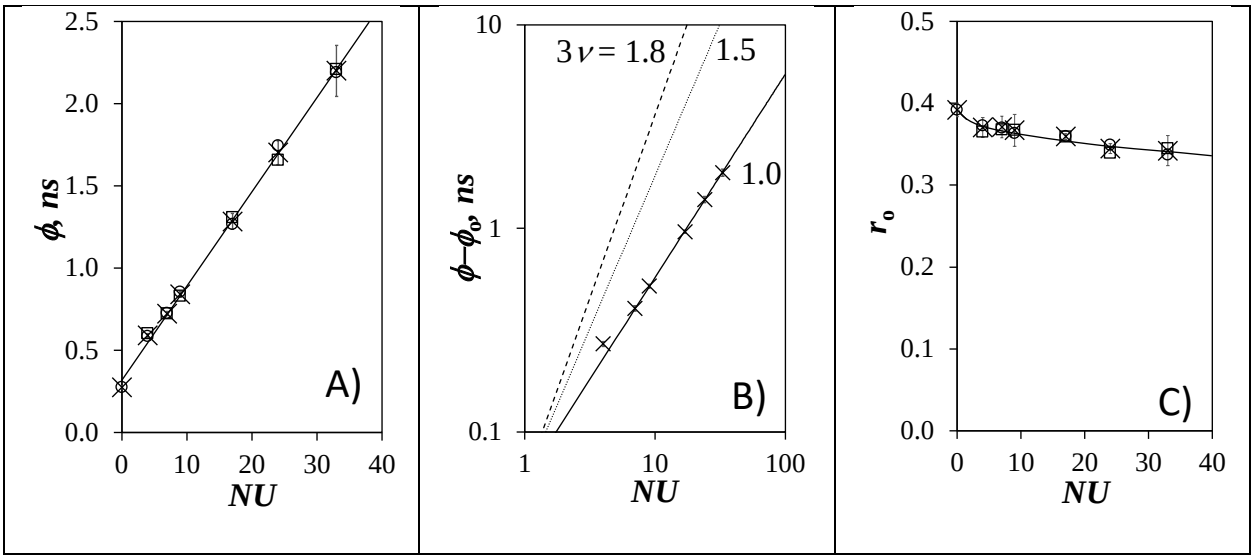

Figure 3.5. A) Plot of the rotational times determined by TRFA as a function of the number of quinoline units constituting a foldamer. B) Log-log plot of $\phi - \phi_o$ as a function of the number of units. (——) $3\nu = 1.0$, (……) $3\nu = 1.5$, (– – –) $3\nu = 1.8$. C) Plot of r_o as a function of the number of quinoline units in the OPV-labeled foldamers. Results from the decays acquired with (○) 10,000 and (□) 20,000 counts; (×) average of all ϕ and r_o values.

Finally, the r_o values corresponding to the anisotropy at $t = 0$ were plotted as a function of *NU* in Figure 3.5C for OPVA and the ester-terminated OPV-Q_n foldamers. The largest r_o value that can be obtained for any dye is 0.4, indicating that the absorption and emission dipole moments of the dye are parallel. The r_o value of OPV equaled 0.39 (±0.01), a value close to 0.4, reflecting that the absorption and emission dipole moments of OPV are parallel, in agreement with earlier reports also stating that both dipole moments are aligned along the main OPV axis.[30,31] As *NU* increased, r_o decreased slightly, indicating a loss of the initial orientation of the dipole moments that occurred on too short a time scale to be probed by the fluorometer. This rapid re-orientation was probably the result of wobbling of the OPV moiety with respect to the helical foldamer. For short *n* values, tumbling of the OPV-Q_n foldamer in solution is determined by the tumbling of the

OPV moiety. However, as *n* increases, it is the foldamer that dictates the tumbling of the OPV, whose wobbling can no longer be transmitted to the entire macromolecule. As a result, the reduction in r_o is believed to reflect some residual loss in the rigidity of the foldamer with increasing chain length.

3.3.4 Anisotropy of rigid symmetric top macromolecules

The trend shown in Figure 3.5 between the rotational time (ϕ) and the number of units (*NU*) of the OPV-Q_n constructs clearly indicates that the progressive addition of quinoline units onto OPV increases the rotational time in a stepwise manner, by relating the increase in ϕ to a commensurate increase in volume of the oligoquinoline foldamer. Yet the simplicity of this result would appear somewhat fortuitous in view of the complex geometry of the OPV-Q_n foldamers. Indeed, helical foldamers are symmetric top macromolecules whose TRFA is best described by the triexponential function given in Equation 3.7.[32]

$$\begin{aligned} r(t) = {} & 0.3\sin^2(\beta_A)\sin^2(\beta_E)\cos(2\xi)\times\exp[-(4D_{//}+2D_{\perp})t] \\ & + 0.3\sin(2\beta_A)\sin(2\beta_E)\cos(\xi)\times\exp[-(D_{//}+5D_{\perp})t) \\ & + 0.1\times[3\cos^2(\beta_A)-1]\times[3\cos^2(\beta_E)-1]\times\exp[-6D_{\perp}t] \end{aligned} \qquad (3.7)$$

A representation of the different parameters used in Equation 3.7 is provided in Figure 3.6 for the three most common symmetric top macromolecules (oblate and prolate ellipsoids, and cylinders). The angles β_A and β_E in Figure 3.6 represent the angles between the absorption and emission dipole moments of the dye with the main axis of the helix, respectively, while the angle ξ corresponds to the angle between the projection of the absorption and dipole moments to the plane perpendicular to the main axis of the symmetric top macromolecule. The tumbling of the

dye solidly bound to the macromolecule in solution results in a triexponential TRFA, whose three rotational times are a function of the two diffusion coefficients $D_{//}$ and $D_{\perp}$.[25,27,32-34] Rotation around the main axis is handled by $D_{//}$, whereas $D_{\perp}$ characterizes the tumbling of the symmetric top macromolecule around the secondary axis of the helix that is perpendicular to the main axis.

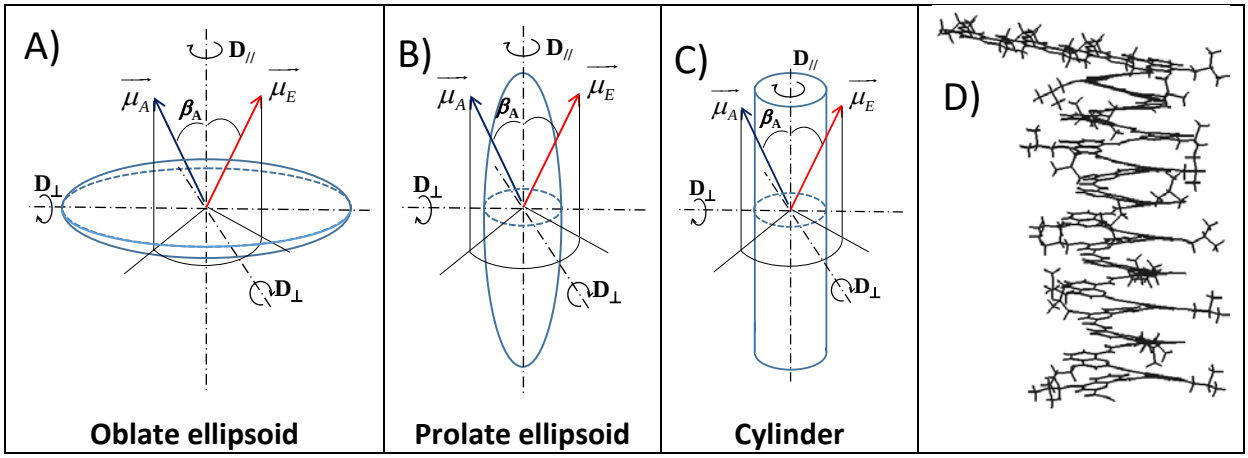

Figure 3.6. Geometries for A) an oblate ellipsoid, B) a prolate ellipsoid, and C) a cylinder. D) Structure of OPV-Q_{24} determined by energy minimization with HyperChem.

Since Equation 3.7 predicts that three different rotational times, namely $\phi_1 = (4\times D_{//}+2\times D_{\perp})^{-1}$, $\phi_2 = (D_{//}+5\times D_{\perp})^{-1}$, and $\phi_3 = (6\times D_{\perp})^{-1}$, are required for the TRFA, of symmetric top molecules, the excellent fits obtained through global analysis of the $I_{VV}(t)$ and $I_{VH}(t)$ decays with Equations 3.1 and 3.2 using a monoexponential TRFA would suggest a problem with the analysis. This apparent contradiction however can be reconciled, by representing the diffusion coefficients $D_{//}$ and $D_{\perp}$ as a function of *NU* in Figure 3.7 for two types of ellipsoids (Ellipsoid-I and Ellipsoid-II), and a cylinder along with the corresponding decay times τ_1, τ_2, and τ_3 that would be obtained in the expressions for $I_{VV}(t)$ and $I_{VH}(t)$ in Equations 3.1 and 3.2, if the TRFA took the form of Equation 3.7.

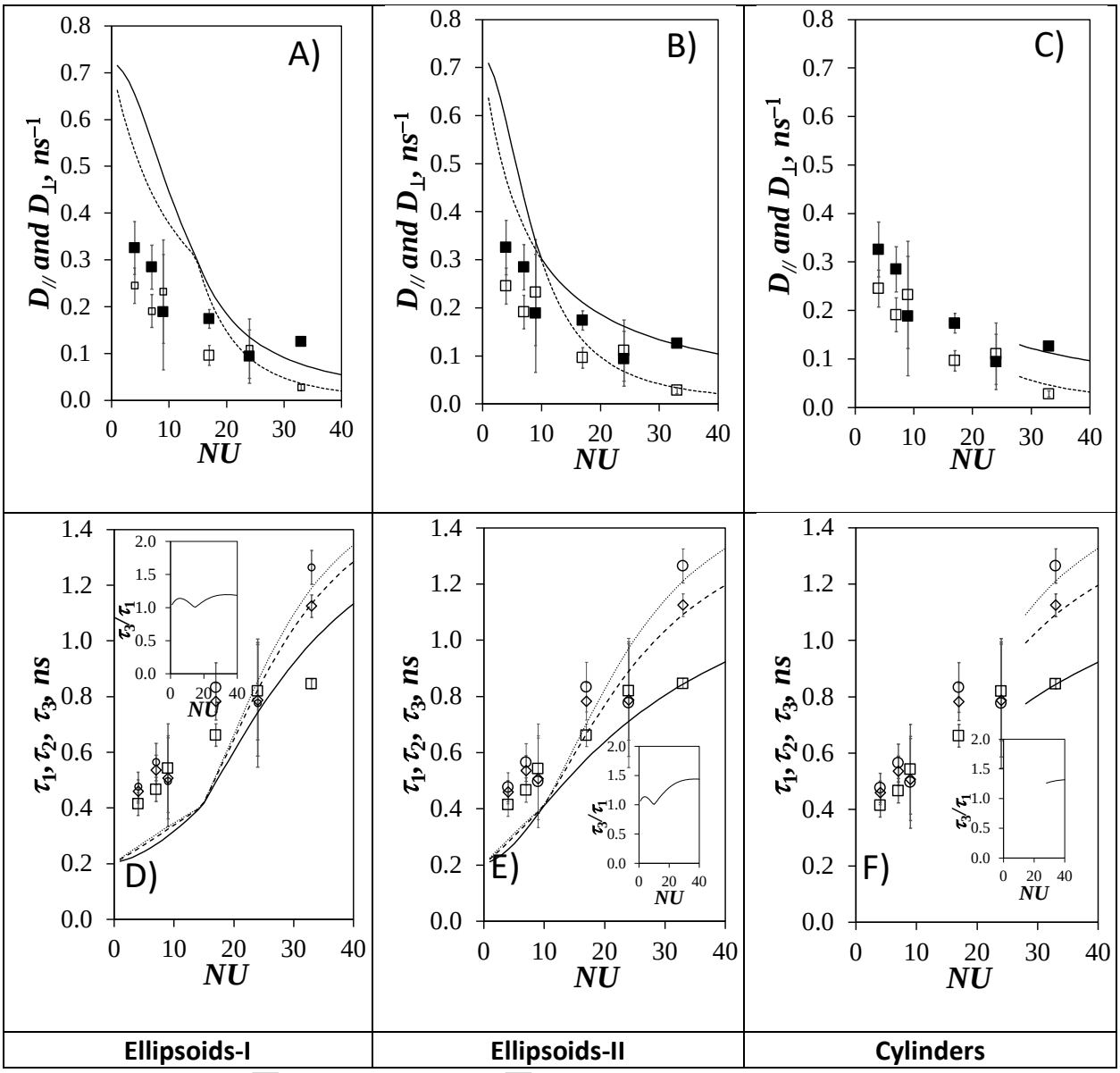

Figure 3.7. Plots of (■, ———) $D_{//}$ and (□, ·····) $D_{\perp}$ as a function of the number of units for A) Ellipsoid-I, B) Ellipsoid-II, and C) Cylinder. Plots of (□, ———) τ_1, (◇, - - - -) τ_2, and (○, ·····) τ_3 as a function of the number of units for D) Ellipsoid-I, E) Ellipsoid-II, and F) Cylinder.The insets represent the ratio τ_3/τ_1 as a function of the number of units.

The calculation of the diffusion coefficients $D_{//}$ and $D_{\perp}$ in Figure 3.7 requires the dimensions of the object along the vertical and horizontal axes, referred to as *L* and *d* for the length

and diameter, respectively. If the macromolecular object was well-described by a cylinder, as would be expected for the helical oligoquinoline foldamers, L would be represented by the product $NU \times \Delta h$ where NU is the number of units constituting the foldamer, Δh is the helical rise per quinoline residue, equal to 0.136 nm, and d would be the helix diameter, estimated to equal 2.0 nm. The aspect ratio ($p = L/d$) is the most important parameter to calculate the diffusion coefficients describing the rotation of a symmetric top macromolecule around its one vertical ($D_{//}$) and two horizontal ($D_{\perp}$) axes of symmetry. As shown hereafter, the diffusion coefficients take different expressions depending on the type of symmetric top macromolecule considered in Figure 3.6.

In the case of an ellipsoid, the diffusion coefficients $D_{//}$ and $D_{\perp}$ are given by Equations 3.8 and 3.9, respectively.[27]

$$D_{//} = \frac{3p(p-S)}{2(p^2-1)} \times \frac{k_B T}{6\eta V_h} \tag{3.8}$$

$$D_{\perp} = \frac{3p[(2p^2-1)S-p]}{2(p^4-1)} \times \frac{k_B T}{6\eta V_h} \tag{3.9}$$

In Equations 3.8 and 3.9, k_B, T, η, and V_h are the Boltzmann constant (1.38×10^{-23} J.K^{-1}), the absolute temperature in Kelvin, the solvent viscosity (0.536 mPa.s for chloroform at 25 ^{o}C), and the hydrodynamic volume of a sphere with a volume equivalent to that of the ellipsoid, respectively. S is a function of p, whose expression given in Equations 3.10 and 3.11, depends on whether the ellipsoid is an oblate ($p < 1$) or a prolate ($p > 1$).

For $p > 1$ (prolate)

$$S = \frac{Ln\left(p + \sqrt{p^2 - 1}\right)}{\sqrt{p^2 - 1}} \tag{3.10}$$

For $p < 1$ (oblate)

$$S = \frac{\arctan\left(\frac{\sqrt{1 - p^2}}{p}\right)}{\sqrt{1 - p^2}} \tag{3.11}$$

Two types of ellipsoids were considered for the calculation of $D_{//}$ and $D_{\perp}$. Ellipsoid-I would have dimensions along the long and short axes given by L and d, representing the helix length (= $NU \times \Delta h$) and diameter (= 2.0 nm), respectively. The volume of Ellipsoid-I with its round tips would thus be smaller than that of a cylinder with sharp tip edges of height L and diameter d, as seen in Figures 3.6B and C. Yet Figure 3.5 suggests that the hydrodynamics of the OPV-Q_n foldamers are well-represented by cylinders whose volume is larger than that of ellipsoids having the same L and d. parameters. To account for this difference, Ellipsoid-II was considered, whose dimension along the secondary axis (perpendicular to the main axis) was given by d equal to 2.0 nm, i.e. the diameter of a helical Q_n foldamer, but whose length L along the main axis was calculated so that its total volume, given by $(\pi/6)Ld^2$, would match that of a cylinder with an NU value equal to n. The $D_{//}$ and $D_{\perp}$ parameters are plotted as a function of the number of quinoline units in Figures 3.7A and B for Ellipsoid-I and Ellipsoid-II, respectively.

In the case of a cylinder, Tirado and Garcia de la Torre derived Equations 3.12 and 3.13 for $D_{//}$ and $D_{\perp}$, respectively, for cylinder aspect ratios ($p = L/d$) between 2 and 30.[33]

$$D_{//} = \frac{k_B T}{A_o \pi \eta L^3}\left(\frac{4p^2}{1 + \delta_{//}}\right) \tag{3.12}$$

$$D_{\perp} = \frac{3k_B T}{\pi \eta L^3}(\ln(p) + \delta_{\perp}) \tag{3.13}$$

In Equations 3.12 and 3.13, A_o equals 3.814, and the functions $\delta_{//}$ and $\delta_{\perp}$ accounting for end-effect corrections due to the cylindrical shape are given in Equations 3.14 and 3.15, respectively.[34]

$$\delta_{//} = 1.119\times10^{-4} + (0.6884/p) - (0.2019/p^2) \quad (3.14)$$

$$\delta_{\perp} = -0.662 + (0.971/p) - (0.050/p^2) \quad (3.15)$$

Using $L = NU\times\Delta h$ where Δh equals 0.136 nm and d = 2.0 nm for the diameter of the cylinder, the $D_{//}$ and $D_{\perp}$ values obtained with Equations 3.12 – 3.15 were plotted as a function of NU in Figure 3.7C. We note that Equations 3.12 – 3.15 are valid as long as the aspect ratio p takes a value between 2.0 and 30, which would correspond to NU values between, respectively, 28 and 441 for the oligoquinoline foldamers.

In order for TRF decay measurements to accurately retrieve decay times from TRF decay analysis, a commonly accepted practice is that every two decay times be separated by at least a factor of 2.[27] The incorporation of Equation 3.7 for the TRFA into Equations 3.1 and 3.2 for the expression of the $I_{VV}(t)$ and $I_{VH}(t)$ decays would result in two tetraexponentials, with one exponential being the longest component equal to the lifetime of the dye (τ_o = 1.6 ns), and the other three decay times τ_1, τ_2, and τ_3, reporting on the rotational times ϕ_1, ϕ_2, and ϕ_3, would be represented by Equations 3.16 – 3.18.

$$\tau_1 = \left(\tau_0^{-1} + \phi_1^{-1}\right)^{-1} = \left(\tau_0^{-1} + 4D_{//} + 2D_{\perp}\right)^{-1} \quad (3.16)$$

$$\tau_2 = \left(\tau_0^{-1} + \phi_2^{-1}\right)^{-1} = \left(\tau_0^{-1} + D_{//} + 5D_{\perp}\right)^{-1} \quad (3.17)$$

$$\tau_3 = \left(\tau_0^{-1} + \phi_3^{-1}\right)^{-1} = \left(\tau_0^{-1} + 6D_{\perp}\right)^{-1} \quad (3.18)$$

The decay times τ_1, τ_2, and τ_3 were then plotted as a function of the number of quinoline units in Figures 3.7D, E, and F for the Ellipsoid-I, Ellipsoid-II, and cylinder geometries, respectively. The ratio τ_3/τ_1 of the largest and the shortest decay times was calculated for each geometry and is plotted in the inset of Figures 3.7D, E, and F. To properly resolve the three decay times τ_1, τ_2, and τ_3, the ratio τ_3/τ_1 would have to be larger than 4, to ensure that τ_2/τ_1 and τ_3/τ_2 be both greater than 2. As shown in the inset of Figures 3.7D – F, the ratio τ_3/τ_1 was never greater than 1.5 for all the geometries considered. This result explains why the $I_{VV}(t)$ and $I_{VH}(t)$ decays could be well-fitted by assuming a monoexponential TRFA instead of the triexponential function given in Equation 3.5, indicating that the recovery of the three decay times τ_1, τ_2, and τ_3 would be challenging.

Despite these poor odds, an attempt was made to improve the resolving power of the fluorescence decay analysis program by adopting the following strategy. First, the $I_{VV}(t)$ and $I_{VH}(t)$ decays were acquired with 20,000 instead of 10,000 counts at the decay maximum, to improve the signal-to-noise ratio. Second, the program analyzed the $I_{VV}(t)$ and $I_{VH}(t)$ decays globally, which notably improves the resolving power of the fluorescence decay analysis program.[35] Third, the program did not optimize the three rotational times ϕ_1, ϕ_2, and ϕ_3 but rather optimized the diffusion coefficients $D_{//}$ and $D_{\perp}$ directly, thus reducing the number of floating parameters from three decay times to two diffusion coefficients. Fourth, the angles β_A, β_E, and ξ, describing the orientation of the absorption and emission dipole moments between themselves and with respect to the frame of the helical foldamer, were estimated through molecular mechanics optimization (MMO) with HyperChem and were used to calculate the pre-exponential factors in Equation 3.7, which were fixed in the analysis of the fluorescence decays. The angle ξ was set to equal zero by noting that since r_o for OPVA equals 0.4 (see Figure 3.5), [30] the absorption and emission dipole moments of

OPV are parallel, thus implying that $\beta_A = \beta_E$ in Figure 3.6. To determine the angle $\beta_A = \beta_E$ between OPV and the main axis of the oligoquinoline helix, the published SCXRD structure of Q_{48} was imported into the modeling program HyperChem.[11] Since the structure of Q_{48} is that of an anhydride between two $Q_{24}A$ moiety, one half of the dimer was deleted because the anhydride moiety induces a small bend in the helix. The OPVA was covalently attached to the N-terminal of Q_{24} *in silico*.[11] Energy minimization of the OPV moiety while fixing the position of all the atoms of Q_{24} yielded the structure shown in Figure 3.6D, where $\beta_A = \beta_E$ was determined to equal 99.5 °. Having determined all the angles needed as inputs in Equation 3.5, Equation 3.19 was obtained for the anisotropy of the OPV-Q_n foldamers.

$$\begin{aligned} r(t) = \; & r_o \times \{\, 0.71 \times \exp[-t \times (4D_{//} + 2D_{\perp})] \\ & + 0.08 \times \exp[-t \times (D_{//} + 5D_{\perp})] \\ & + 0.21 \times \exp[-t \times (6D_{\perp}]\} \end{aligned} \qquad (3.19)$$

The advantage of using Equation 3.19 as compared to Equation 3.7, with three floating rotational times and three floating pre-exponential factors, was to reduce the number of floating parameters from 6 to 3, namely r_o, $D_{//}$, and $D_{\perp}$. All $I_{VV}(t)$ and $I_{VH}(t)$ decays acquired with 20,000 counts at the decay maximum were fitted by inputting Equation 3.19 into Equations 3.1 and 3.2. The recovered decay times τ_1, τ_2, and τ_3, and diffusion coefficients $D_{//}$ and $D_{\perp}$ were plotted as a function of the number of units in Figure 3.5. For all OPV-Q_n constructs, the τ_1, τ_2, and τ_3 decay times clustered together, as would be expected from these objects having a small aspect ratio ($p <$ 2.2) and as found experimentally, since a single rotational time was sufficient in Equation 3.3 to fit the $I_{VV}(t)$ and $I_{VH}(t)$ decays. Only in the case of the longest OPV-Q_{33} sample did the $D_{//}$ and $D_{\perp}$

diffusion coefficients and τ_1, τ_2, and τ_3 decay times line up with the trends expected for an Ellipsoid-II or Cylinder geometry. The decay times retrieved for the smaller ellipsoids representing the shorter helical foldamers were longer than expected, thus indicating longer rotational times. These longer rotational times were probably due to the 18.7 Å long and 8.7 Å wide OPV moiety, as determined from MMO conducted with HyperChem. Considering its ϕ value of 0.27 ns, OPVA would have a hydrodynamic volume of 2.1 nm^3, equivalent to that of a pentaquinoline foldamer. OPVA will thus slow down the diffusion of the shorter foldamers, but its effect should decrease with increasing foldamer length, becoming negligible for the longer foldamers with 20 or more oligoquinolines, where the OPVA volume represents less than 20% of the overall volume of the macromolecule.

While it is clear that the dimension of the fluorescent OPV label affects the rotational time of the OPV-Q_n foldamers, particularly for low NU, this effect is much more difficult to handle quantitatively in the case of symmetric top geometries. As observed in Figure 3.5A, where the geometry of the OPV-Q_n foldamers was approximated to that of a sphere, the effect of the finite volume of the OPV-label manifested itself simply as a the non-zero intercept for the straight line. Every quinoline addition contributed a set volume to the hydrodynamic volume of the OPV-Q_n foldamer, resulting in the simple straight line found in Figure 3.5A. Although not mathematically correct, the representation of the foldamers as spherical objects appears to be fully justified for OPV-Q_n foldamers with $1 < n < 33$ based on the trends generated in Figure 3.8, that demonstrate that the rotational times retrieved by assuming a symmetric top geometry for these objects would result in three similar rotational times, that are challenging to resolve experimentally.

3.3 Conclusions

It was demonstrated in this chapter that TRFA is ideally suited to probe the hydrodynamic behavior of rigid foldamers in solution. It was applied to a series of OPV-Q_n foldamers, whose rotational time was found to increase linearly with increasing foldamer length. This result is taken as evidence that the addition of one quinoline residue increases the hydrodynamic volume of the foldamer by a set amount, as would be expected for rigid helical objects. Furthermore, the hydrodynamic volume of the OPV-Q_n constructs matches perfectly that expected from the dimensions of oligoquinoline helices in the solid state retrieved from SCXRD. The excellent agreement between the structural information retrieved for the foldamers in the solid state by SCXRD and in solution by TRFA is evidence of the reliability of TRFA to probe the structure of rigid foldamers in solution. Consequently, this study opens the path to the use of TRFA in the characterization of foldamers in solution.

Chapter 4

Application of TRFA to probe foldamer self-assembly via metal coordination

4.1 Introduction

Unpublished work from the H-Lab in Bordeaux suggested that metal coordination of the terminal carboxylate anions of the foldamers yields larger foldamer complexes. Consequently, this procedure might offer an exciting non-synthetic pathway towards foldamer elongation. However, validation of this foldamer elongation procedure depends critically on one's ability to probe the dimension of the putative foldamer complexes in solution. The sensitivity of TRFA to macromolecular size established in Chapter 3 led to the selection of this technique to probe the dimensions of the metal complexes generated by the OPV-Q_nA foldamers. In this chapter, OPV-Q_4A, OPV-Q_8A, Q_8A, Q_{16}A, OPV-Q_{17}A, and OPV-Q_{33}A were employed to form the metal complexes referred to as (OPV-Q_4A)$_2$-Na, (OPV-Q_8A)$_2$-Na, OPV-Q_8A-Na-Q_8A, OPV-Q_8A-Na-Q_{16}A, OPV-Q_{17}A-Na-Q_8A, (OPV-Q_{17}A)$_2$-Na, OPV-Q_{33}A-Na-Q_8A, OPV-Q_{33}A-Na-Q_{16}A and (OPV-Q_{33}A)$_2$-Na where the overall number of units was expected to equal 8, 16, 16, 24, 25, 34, 41, 49, and 66, respectively. TRFA measurements of each metal complex samples were conducted in the same manner as described in Chapter 3. However, as the foldamer length increased, the geometry of the foldamer could no longer be approximated by that of an isotropic object and the $I_{VV}(t)$ and $I_{VH}(t)$ of the longer constructs could not be satisfyingly fitted by assuming a monoexponential TRFA as had been done in Chapter 3 for the shorter OPV-Q_n foldamers with *n*

≤ 33. Analysis of the $I_{VV}(t)$ and $I_{VH}(t)$ decays obtained for the longer constructs required that all the TRFA took into account the symmetric top geometry associated with a cylindrical shape for the foldamer complexes as well as wobbling of the OPV dye with respect to the frame of these constructs.

4.2 Experimental

4.2.1 Materials

Chloroform (HPLC grade) was used as received in all fluorescence experiments. Sodium hydroxide was bought from Sigma-Aldrich and was reagent grade. The doubly distilled Mili-Q water used to prepare the metal complexes was obtained from a Millipore Milli-RO 10 Plus or Milli-Q UFPlus, Bedford, MA system. The Q_nA, OPV-Q_nA and AQ_2PQ_2A samples used in this study were prepared by Dr. Victor Maurizot from the University of Bordeaux, France. Their chemical structure is presented in Figure 4.1 and their preparation has been reported earlier.[10,26]

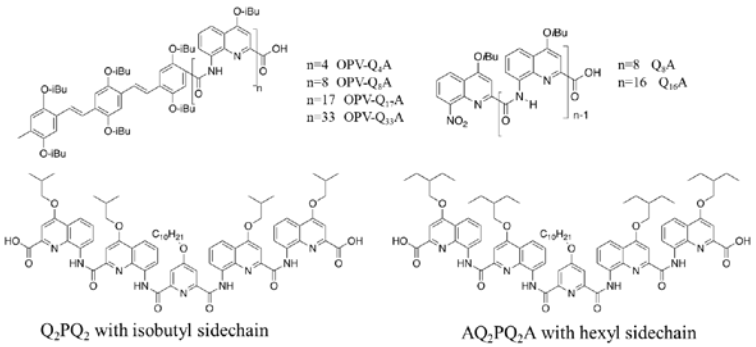

Figure 4.1. Chemical structure of Q_nA, OPV-Q_nA and AQ_2PQ_2A.

4.2.2 Preparation of the metal complex foldamer.

The $(OPV\text{-}Q_nA)_2$-Na complexes were obtained by adding one NaOH pellet into 4 mL of a 1.4×10^{-5} M OPV-Q_nA chloroform solution in the presence of 0.05 mL of water and stirring the mixture for 10 min. Similarly, the OPV-Q_nA-Na-Q_mA complexes were generated by adding a solid NaOH pellet and 0.05 mL of water to a 4 mL chloroform solution containing 2.8×10^{-5} M OPV-Q_nA and 2.8×10^{-4} M Q_mA and stirring the mixture vigorously for 10 min. The 10-fold excess of Q_mA used in these mixtures was meant to maximize the probability that all the fluorescently labeled OPV-Q_nA form a complex. After allowing the aqueous phase to separate from the organic phase, the foldamer solution in chloroform was withdrawn and placed in a fluorescence cell to conduct fluorescence measurements.

4.2.3 Dilution test on OPV-Q_8A and Q_{16}A mixtures.

Several solutions of 1:10 OPV-Q_8A:Q_{16}A mixture were prepared in chloroform where the concentration of OPV-Q_8A was progressively diluted from 1.5 to 0.15 μM. One NaOH pellet and 0.05 mL of water were added to 4 mL of foldamer solution in chloroform. After vigorous stirring for 10 min and allowing the separation of the chloroform and aqueous phase, the foldamer solution was transferred to a fluorescence cell.

4.2.4 Polymerization of AQ_2PQ_2A with OPV-Q_8A stoppers

AQ_2PQ_2A with isobutyl side chains was dissolved in chloroform at concentrations ranging from 17 to 136 μM, while chloroform solutions of AQ_2PQ_2A with hexyl side chains were prepared at concentrations ranging from 17 to 510 μM. A 4 mL solution of a given AQ_2PQ_2A concentration was prepared in chloroform with a fixed 16 μM OPV-Q_8A concentration to yield solutions with different AQ_2PQ_2A:OPV-Q_8A ratios. Then, one NaOH pellet and water (0.05 mL) were added into

the chloroform solution and the mixture was stirred for 10 min to induce the polymerization of AQ_2PQ_2A with OPV-Q_8A stoppers through their complexation.

4.2.5 Absorption and fluorescence measurements and analysis of the fluorescence decays

The same instruments and protocols described in the Experimental section of Chapter 3 were employed in Chapter 4. The equations from Chapter 3 that are most relevant to the analysis of the fluorescence decays conducted in Chapter 4 are briefly reviewed hereafter. The fluorescence decays acquired with a vertically polarized excitation and a vertically ($I_{VV}(t)$) and horizontally ($I_{VH}(t)$) polarized emission were fitted globally according to Equations 4.1 and 4.2, respectively. To qualify as good, a fit was required to result in a χ^2 value of less than 1.30, and to yield residuals and autocorrelation of residuals randomly distributed around zero.

$$I_{VV}(t) = \frac{I_o}{3} e^{-t/\tau_o} \times (1 + 2r(t)) \tag{4.1}$$

$$I_{VH}(t) = \frac{I_o}{3G} e^{-t/\tau_o} \times (1 - r(t)) \tag{4.2}$$

In Equations 4.1 and 4.2, the function $r(t)$ is the TRFA.[27] The TRFA was well represented by the single exponential shown in Equation 4.3, where ϕ and r_o are the rotational time and initial anisotropy, respectively, for OPV-Q_nA complexes with overall dimensions smaller than an equivalent OPV-Q_n foldamer with $n < 40$.

$$r(t) = r_o e^{-t/\phi} \tag{4.3}$$

For larger objects, poor fits were obtained when Equation 4.3 was used for the TRFA. These larger objects were assumed to adopt a cylindrical conformation resulting in Equation 4.4 for the TRFA.[32]

$$r(t)=\frac{r_o}{0.3\sin^2(\beta_A)\sin^2(\beta_E)\cos(2\xi)+0.3\sin(2\beta_A)\sin(2\beta_E)\cos(\xi)+0.1[3\cos^2(\beta_A)-1][3\cos^2(\beta_E)-1]}\times$$

$$\begin{aligned}&\{0.3\sin^2(\beta_A)\sin^2(\beta_E)\cos(2\xi)\times\exp[-(4D_{//}+2D_{\perp})t]\\&+0.3\sin(2\beta_A)\sin(2\beta_E)\cos(\xi)\times\exp[-(D_{//}+5D_{\perp})t)\\&+0.1\times[3\cos^2(\beta_A)-1]\times[3\cos^2(\beta_E)-1]\times\exp[-6D_{\perp}t]\}\end{aligned}\qquad(4.4)$$

Consequently, the anisotropy in Equation 4.4 is a sum of three exponentials with the rotational times ϕ_1, ϕ_2, and ϕ_3 whose expression is given in Equations 4.5 – 4.7.

$$\phi_1=\left(4D_{//}+2D_{\perp}\right)^{-1}\qquad(4.5)$$

$$\phi_2=\left(D_{//}+5D_{\perp}\right)^{-1}\qquad(4.6)$$

$$\phi_3=\left(6D_{\perp}\right)^{-1}\qquad(4.7)$$

In Equations 4.4 – 4.7, the diffusion coefficients $D_{//}$ and $D_{\perp}$ represent the rotation of the cylinder around its main and secondary axis, respectively, β_A and β_E are the angles between the major axis of the cylinder and the dipole moments of absorption (μ_A) and emission (μ_E) of the dye, respectively, and ξ is the angle between the projection of μ_A and μ_E in the plane perpendicular to the major axis of the cylinder (see Figure 3.6C).[32] In the case of the OPV-Q_n foldamers, the angles ξ, β_A, and β_E have been found to equal 0, 99.5, and 99.5 °, respectively, so that r_o should equal 0.4.

An r_o value lower than 0.4 implies that OPV undergoes isotropic wobbling that occurs on a timescale that is too short for detection with the time-resolved fluorometer.[37]

The conclusion reached in an earlier study that the OPV-Q_n foldamer could be viewed as cylindrical objects suggested that Equations 4.8 – 4.11, derived by Tirado and Garcia de la Torre, could be applied to estimate the diffusion coefficients $D_{//}$ and $D_{\perp}$ of the foldamers.[33]

$$D_{//} = \frac{k_B T}{A_o \pi \eta L^3}\left(\frac{4p^2}{1+\delta_{//}}\right) \tag{4.8}$$

$$D_{\perp} = \frac{3k_B T}{\pi \eta L^3}(\ln(p) + \delta_{\perp}) \tag{4.9}$$

Equations 4.8 and 4.9 are valid for aspect ratios $p = L/d$, where L and d are the length and the diameter of the helical foldamer, respectively, between 2 and 30. These equations use the parameter A_o equal to 3.814 and the functions $\delta_{//}$ and $\delta_{\perp}$ that account for end-effect corrections due to the cylindrical shape. The expressions of $\delta_{//}$ and $\delta_{\perp}$ are given in Equations 4.10 and 4.11, respectively.

$$\delta_{//} = 1.119\times10^{-4} + (0.6884/p) - (0.2019/p^2) \tag{4.10}$$

$$\delta_{\perp} = -0.662 + (0.971/p) - (0.050/p^2) \tag{4.11}$$

Considering that $L = NU\times\Delta h$ where Δh equals 0.136 nm and d = 2.0 nm for the diameter of the cylinder, and that the aspect ratio p can only take values between 2.0 and 30, it implies that the diffusion coefficients $D_{//}$ and $D_{\perp}$ can only be determined for foldamers with NU values between

28 and 441, respectively. Equation 4.4 could be used to determine the number-average rotational time (<ϕ>) of the object as shown in Equation 4.12, which was used to characterize its dimensions.

$$<\phi>=\frac{\frac{0.3\sin^2(\beta_A)\sin^2(\beta_E)\cos(2\xi)}{4D_{//}+2D\perp}+\frac{0.3\sin(2\beta_A)\sin(2\beta_E)\cos(\xi)}{D_{//}+5D_{\perp}}+\frac{0.1[3\cos^2(\beta_A)-1][3\cos^2(\beta_E)-1]}{6D_{\perp}}}{0.3\sin^2(\beta_A)\sin^2(\beta_E)\cos(2\xi)+0.3\sin(2\beta_A)\sin(2\beta_E)\cos(\xi)+0.1[3\cos^2(\beta_A)-1][3\cos^2(\beta_E)-1]} \quad (4.12)$$

4.3 Results and Discussion

4.3.1 Rotational time of metal complexes

All pairs of I_{VV}(t) and I_{VH}(t) decays, acquired for the complexes containing at least one OPV-Q_nA segment, were globally analyzed by first assuming a monoexponential TRFA as described in Equation 4.1 using the program *aniso01d-4*, which optimized r_o, ϕ, the lifetime (τ_o) of the dye, and the G-factor. The ϕ values of the foldamer complexes retrieved from this analysis are plotted in Figure 4.2 against their expected number of units. The solid straight line in Figure 4.2 represents the linear relationship obtained in Chapter 3 between the rotational time of the OPV-Q_n foldamers and their number of units, given as Equation 4.13. Within experimental error, the rotational times of the OPV-Q_nA foldamers terminated with a carboxylic acid at one end clustered around the straight line, indicating that the nature of the C-terminal of the Q_n foldamer, whether it was a carboxylic acid for OPV-Q_nA or a methyl ester for OPV-Q_n, had little effect on the tumbling of the macromolecules in solution.

$$\phi = 0.057\times NU + 0.32 \quad (4.13)$$

The rotational time of the OPV-Q_mA-Na-Q_nA complexes was also plotted in Figure 4.2 as a function of the number of units expected for a foldamer made of $n+m$ quinolines. The rotational time increased linearly with increasing number of units and fell on the calibration curve for numbers of units lower than 41. For longer foldamers, ϕ reached a plateau at around 2.5 ns. When NU was lower than 41, the rotational time of the complexes corresponded to an equivalent foldamer having an NU value equal to the sum of the NUs of the constituting foldamers; in other words, the rotational time of the OPV-Q_mA-Na-Q_nA complex was equal to the rotational time of OPV-Q_{m+n}. This result strongly suggests that the complexation of two foldamers in solution generated a fully stacked foldamer. Unfortunately, this nice correlation breaks down for longer foldamers with *NU* greater than 41, whose rotational time appears to plateau when the TRFA was assumed to be monoexponential (Equation 4.3).

The deviation of ϕ from the straight line in Figure 4.2 for larger foldamer complexes might simply reflect the inability of a monoexponential TRFA to describe a symmetric top macromolecule with a large aspect ratio such as that of an OPV-Q_{66} foldamer, that would be equivalent to an (OPV-Q_{33}A)$_2$-Na dimer. Although global analysis with *aniso01d-4* of the $I_{VV}(t)$ and $I_{VH}(t)$ fluorescence decays of (OPV-Q_nA)$_2$-Na assuming a monoexponential TRFA yielded a χ^2 value of 1.27, smaller than the recommended value of 1.30, the residuals and autocorrelation of the residuals were not perfectly randomly distributed around zero in Figure 4.2A and B. The non-random distribution of the residuals and their autocorrelation function in Figure 4.2A suggests a poor fit, in agreement with the notion that a monoexponential TRFA was not suited to represent the larger foldamer complexes.

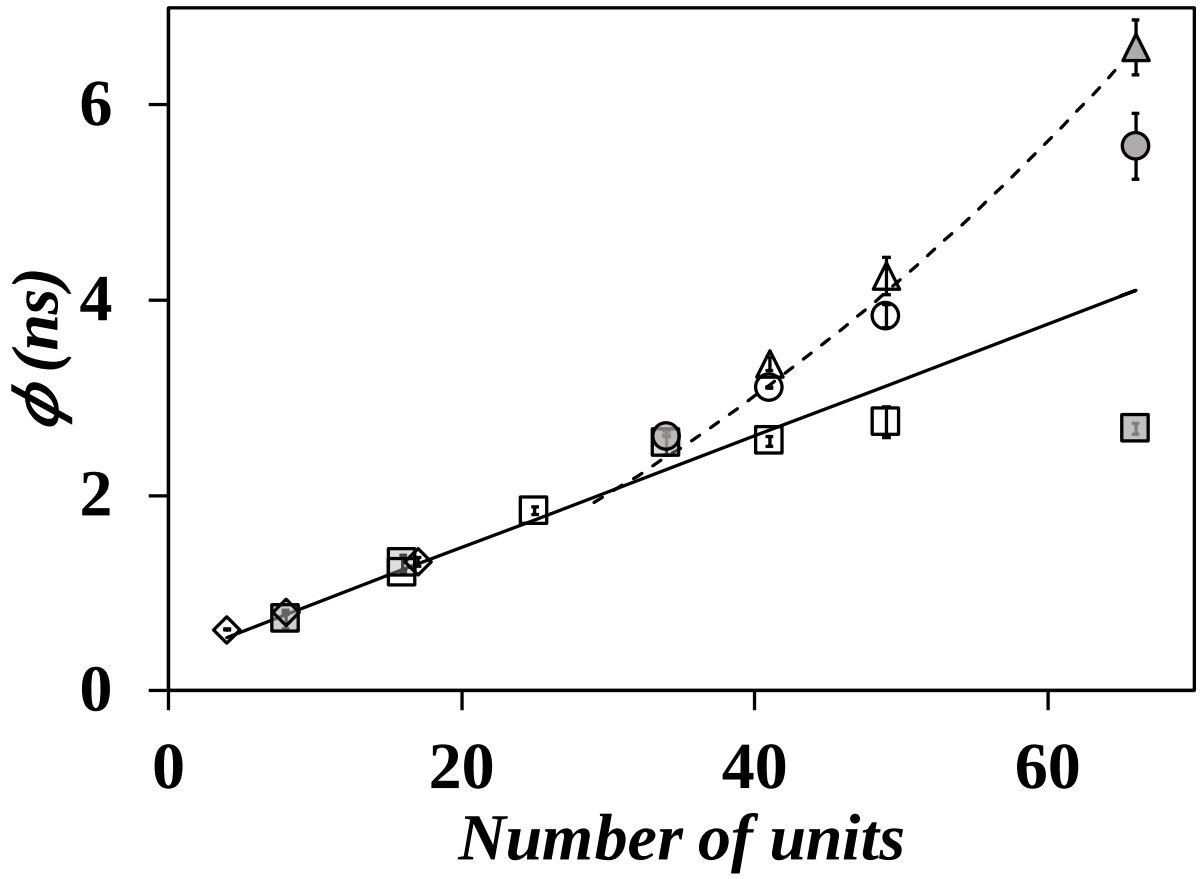

Figure 4.2. Plot of the rotational times of OPV-Q_nA (◇) and metal complexes determined by aniso01d-4 (□), aniso02o-3 (○), and aniso03c (△). Grey and empty symbols represent the (OPV-Q_nA)$_2$-Na dimers bearing two OPVs and the OPV-Q_mA-Na-Q_nA complexes with only one OPV, respectively. Rotational times according to (– –) Equation 4.12 and (—) Equation 4.13 .

One obvious reason for the worsening of the fits for larger OPV-Q_nA complexes could be their larger aspect ratio $p = L/d$ that would equal 2.8, 3.3, and 4.5 for the OPV-Q_{33}A-Na-Q_8A, OPV-Q_{33}A-Na-Q_{16}A, and (OPV-Q_{33}A)$_2$-Na complexes, respectively. For such large aspect ratios, the difference in $D_{//}$ and $D_{\perp}$ might be too large and result in rotational times ϕ_1, ϕ_2, and ϕ_3 in Equations 4.5 – 4.7 too different to approximate the tri-exponential TRFA shown in Equation 4.4,

with the single exponential TRFA given in Equation 4.3. As shown in Figure 4.4A, the ratio $D_{//}/D_{\perp}$ increases from 2.2 to 6.3 when the number of units of a helical foldamer increases from 30 to 70 and the rotational times ϕ_1, ϕ_2, and ϕ_3 diverge dramatically in Figure 4.4B, thus rationalizing the failure of a monoexponential TRFA to fit the $I_{VV}(t)$ and $I_{VH}(t)$ decays of the longer foldamer complexes. Consequently, Equation 4.4 was employed to fit the $I_{VV}(t)$ and $I_{VH}(t)$ decays globally with Equations 4.1 and 4.2. However, before conducting the fits, the rotational times ϕ_1, ϕ_2, and ϕ_3 given in Equations 4.5 – 4.7 were used to determine the decay times τ_1, τ_2, and τ_3 given in Equations 4.14 – 4.16, that would need to be differentiated in the decay analysis.

$$\tau_1 = \left(\phi_1^{-1} + \tau_o^{-1}\right)^{-1} \tag{4.14}$$

$$\tau_2 = \left(\phi_2^{-1} + \tau_o^{-1}\right)^{-1} \tag{4.15}$$

$$\tau_3 = \left(\phi_3^{-1} + \tau_o^{-1}\right)^{-1} \tag{4.16}$$

The trends obtained with the decay times plotted in Figure 4.4C indicate that τ_3 is much too close to τ_o to be retrieved accurately. As a rule of thumb, two decay times can be retrieved with confidence from a multiexponential fit of fluorescence decays if one of the decay times is at least twice larger than the other decay time.[27] As indicated in Figure 4.4C, this condition is clearly not obeyed for the three decay times τ_1, τ_2, and τ_3, among themselves and as compared to τ_o. Consequently, the following strategy was applied to fit the decays. Since the angles ξ, β_A, and β_E were known to equal 0, 99.5, and 99.5 ^{o}, the pre-exponential factors in Equation 4.4 were fixed to their values during the decay analysis. Instead of optimizing the decay times τ_1, τ_2, and τ_3, the analysis program optimized the diffusion coefficient $D_{//}$, while $D_{\perp}$ was fixed to the value expected

from a foldamer of size equivalent to that of a given foldamer complex. In so doing, the program *aniso02o-3* optimized r_o, $D_{//}$, τ_o, and the *G*-factor as had been done earlier, reducing the number of floating parameters.[37]

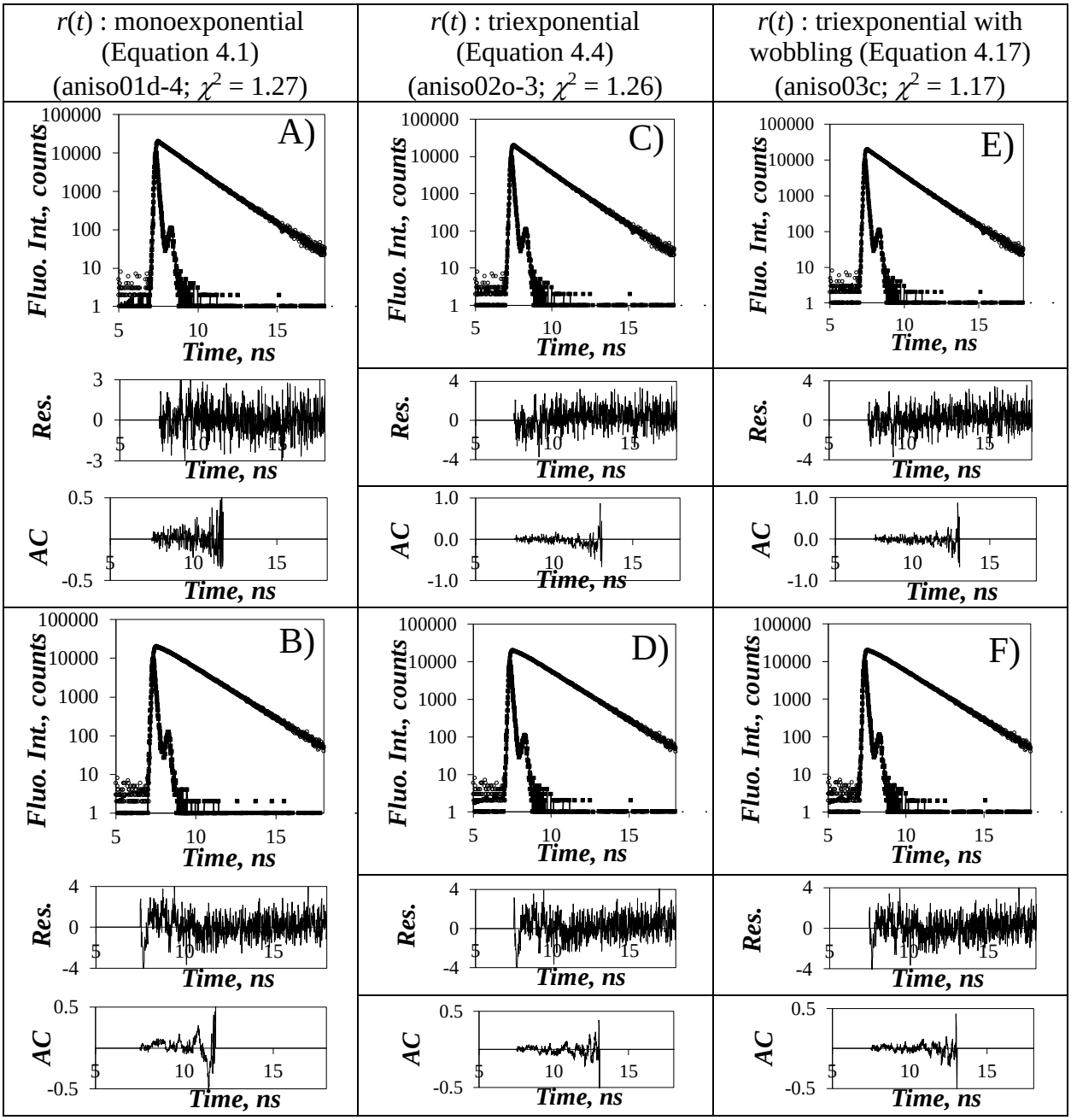

Figure 4.3. Examples of fits from the global analysis of the A), C), and E) $I_{VV}(t)$ and B), D), and F) $I_{VH}(t)$ decays of (OPV-Q_{33}A)$_2$-NA dimers in chloroform with the programs A) and B) *aniso01d-4*, C) and D) *aniso02o-3*, and E) and F) *aniso03c*.

With the diffusion coefficients $D_{//}$ and $D_{\perp}$ being, respectively, optimized and fixed in the analysis, the averaged rotational time $<\phi>$ was calculated according to Equation 4.12 and plotted in Figure 4.2 as a function of the number of quinolines. Although $<\phi>$ approaches the trend shown as a dashed line in Figure 4.2, expected for cylinders, it still underestimates the expected value. However, using Equation 4.4 instead of Equation 4.3 only marginally improved the quality of the fit, with χ^2 decreasing from 1.27 to 1.26 in Figure 4.3C and D. Furthermore, the fits of the $I_{VV}(t)$ and $I_{VH}(t)$ decays show clear distortions at early times. These distortions occurring on a fast time scale suggest wobbling of OPV with respect to the frame of the foldamer complex.

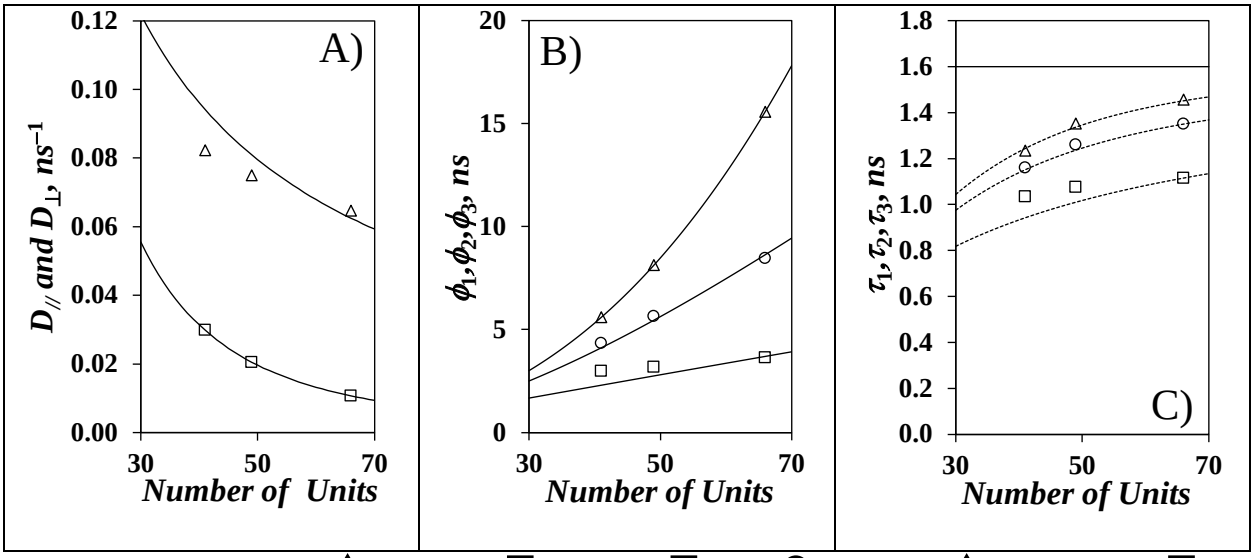

Figure 4.4. Plots of A) (△) $D_{//}$ and (□) $D_{\perp}$, B) (□) ϕ_1, (○) ϕ_2, and (△) ϕ_3, and C) (□) τ_1, (○) τ_2, and (△) τ_3 obtained with *aniso03c* as a function of the number of units. The lines that pass closest to the symbols are the trends based on $D_{//}$ and $D_{\perp}$ calculated from Equations 4.8 – 4.11. Solid horizontal line in C) represents τ_o = 1.6 ns.

OPV wobbling could be handled by using Equation 4.17, derived by Duhamel et al,[25] by assuming that wobbling of the dye occurs between two reflecting barriers making an angle l between them, $\omega(p) = p\pi/l$, and D_w is the rotational diffusion coefficient for the wobbling of OPV around the helical axis. If anisotropic wobbling occurs on a fast time scale that cannot be observed with the fluorometer it would be handled by r_o. The analysis program *aniso03c* used Equation 4.17 to fit globally the $I_{VV}(t)$ and $I_{VH}(t)$ fluorescence decays, where r_o, $D_{//}$, D_w, τ_o, and the G-factor were optimized for a given l value which was fixed in the analysis. Varying l in 5 ^{o} increments resulted in an optimal fit, as shown in Figure 4.3E and F, where the residuals and autocorrelation of the residuals were better distributed around zero and the χ^2 showed a substantial improvement by decreasing from 1.26 to 1.17. The average rotational time calculated from the $D_{//}$ and $D_\perp$ values clustered around the dashed line predicted for a cylindrical geometry in Figure 4.2, suggesting that proper handling of the TRFA requires accounting for wobbling and the two diffusion coefficients $D_{//}$ and $D_\perp$.

$$r(t) = \frac{r_o}{0.3\sin^2(\beta_A)\sin^2(\beta_E)\cos(2\xi) + 0.3\sin(2\beta_A)\sin(2\beta_E)\cos(\xi) + 0.1[3\cos^2(\beta_A)-1][3\cos^2(\beta_E)-1]} \times$$

$$\left\{0.3\sin^2(\beta_A)\sin^2(\beta_E)\cos(2\xi)\times\exp[-(4D_{//}+2D_\perp)t]\times\right.$$

$$\left[\frac{\sin^2 l}{l^2} + \frac{1}{l^2}\sum_{p=1}^{\infty}\frac{1-(-1)^p\cos 2l}{\left[1-\omega^2(p)/4\right]^2}\exp\left[-\omega^2(p)D_w t\right]\right]$$

$$+0.3\sin(2\beta_A)\sin(2\beta_E)\cos(\xi)\times\exp[-(D_{//}+5D_\perp)t)\times$$

$$\left[\frac{\sin^2(l/2)}{(l/2)^2}+\frac{1}{(l/2)^2}\sum_{p=1}^{\infty}\frac{1-(-1)^p\cos(l)}{\left[1-\omega^2(p)\right]^2}\exp\left(-\omega^2(p)D_w t\right)\right]$$

$$+0.1\times[3\cos^2(\beta_A)-1]\times[3\cos^2(\beta_E)-1]\times\exp[-6D_\perp t]\Big\} \qquad (4.17)$$

In summary, several analysis programs were implemented and their ability to fit globally the $I_{VV}(t)$ and $I_{VH}(t)$ decays obtained with the foldamer complexes was assessed. In the end, an analysis that included wobbling of the OPV and the two diffusion coefficients for symmetric top macromolecules could successfully probe the size of foldamer complexes equivalent to an OPV-Q_{66} oligoquinoline. Based on these results, metal coordination of oligoquinoline foldamer acids would appear to be a reliable method to elongate quinoline-based foldamers.

4.3.2 r_o values of metal complexes

The r_o values retrieved by the three different analysis programs, used to fit the $I_{VV}(t)$ and $I_{VH}(t)$ decays, were plotted as a function of the number of units of the foldamers in Figure 4.5. In general, the r_o values retrieved by assuming a monoexponential TRFA (Equation 4.3), a triexponential TRFA (Equation 4.4), and a triexponential TRFA with wobbling (Equation 4.17) were lowest, intermediate, and highest, respectively. The differences between the r_o values increased with increasing foldamer length, as longer foldamers required increasingly complex expressions for the TRFA to handle the cylindrical geometry of these symmetric top macromolecules and the wobbling of the OPV. When all the different decorrelation processes were accounted for with the program *aniso03c*, r_o took its largest value equal to 0.35 ± 0.01. Since the two other programs did not formally account for the more rapid decorrelation processes, they yielded lower r_o values to reflect this rapid decorrelation.

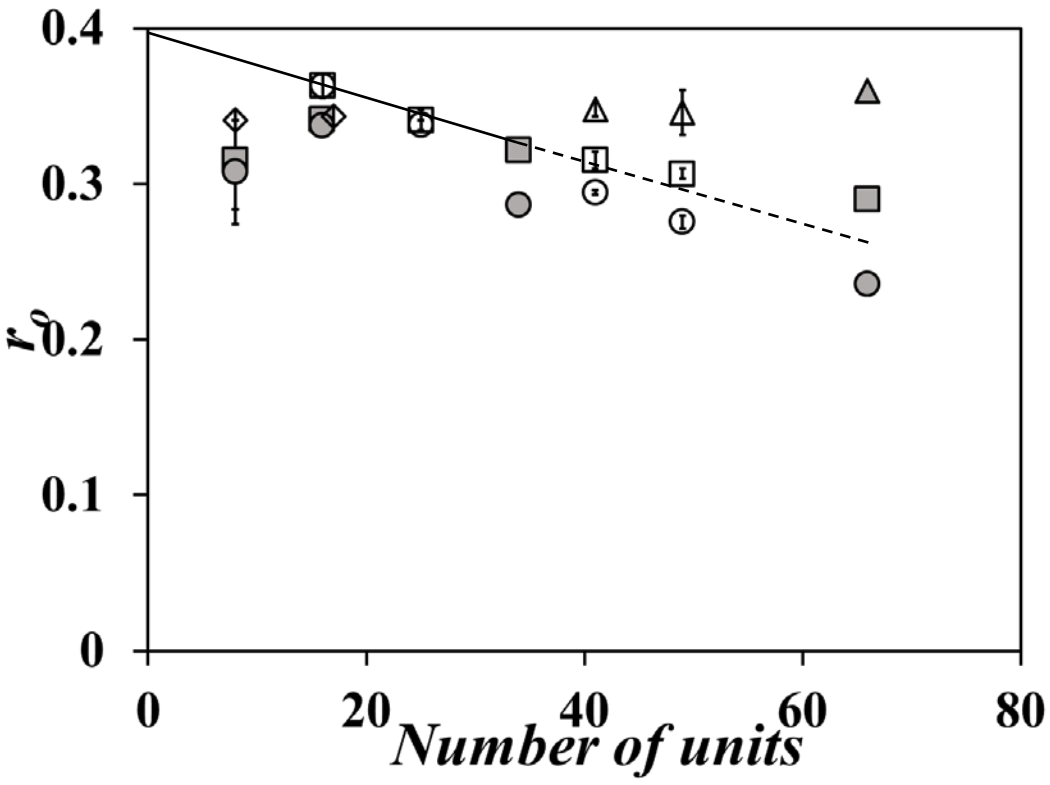

Figure 4.5. Plot of r_o of OPV-Q_nA (◇) and metal complexes determined by *aniso01d-4* (○), *aniso02o-3* (□), and *aniso03c* (△). Grey and empty symbols represent the (OPV-Q_nA)$_2$-Na dimers bearing two OPVs and the OPV-Q_mA-Na-Q_nA complexes with only one OPV, respectively. (▬) r_o values obtained for the OPV-Q_n foldamers using Equation 4.3 for $r(t)$ up to n = 33 and (…) extrapolation for longer OPV-Q_n foldamers.

While the different trends obtained with r_o could be rationalized based on the ability of the analysis programs to account for the various decorrelation processes, the low r_o value obtained for the (OPV-Q_4A)$_2$-Na complex was somewhat surprising. This complex, which was expected to have a rotational time similar to that of OPV-Q_8, should have been short enough for a monoexponential TRFA. Although the fits appeared satisfactory, the retrieved r_o value of 0.31 ± 0.03 was substantially lower than that of 0.37 expected for OPV-Q_8. Since r_o equals

$0.2\times(3\cos^2(\alpha)-1)$, where α is the angle between the absorption and emission dipole moments, an r_o value of 0.31 would be equivalent to an α value of 23 or 157 °, rather than 0 ° as found in this thesis and other studies for OPV.[36] Since the (OPV-Q_4A)$_2$-Na complex was relatively short and contained two OPV moieties, the possibility of having energy hopping between the two OPV moieties was considered. Rapid energy hopping between the two dyes would lead to the instantaneous delocalization of the absorption and emission dipole moments, that could result in the apparent decrease in r_o observed for this complex.

The efficiency of fluorescence resonance energy transfer (FRET) between the two dyes can be characterized by determining the Förster radius (R_o), whose expression is given in Equation 4.18. In a typical FRET experiment, the integral in Equation 4.18 describes the overlap between the fluorescence spectrum of the donor and the absorption spectrum of the acceptor. In the present case where the donor and acceptor are two OPV labels on the same molecule, the integral represents the overlap between the absorption and fluorescence spectra of OPVA shown in Figure 3.2. In Equation 4.18, Φ_{OPV} is the quantum yield of OPVA, found to equal 0.62 ± 0.04, N_A is the Avogadro number, n is the refractive index of the solvent, $F_{OPV}(\lambda)$ is the normalized fluorescence intensity of OPVA, $\varepsilon_{OPV}(\lambda)$ is the extinction coefficient of OPVA, and κ^2 is the orientation factor describing the relative orientation in space of the transition dipoles of the donor and the acceptor, whose expression is given in Equation 4.19.

$$R_o = \frac{9000Ln(10)\kappa^2\Phi_{OPV}}{128\pi^5 N_A n^4}\int_0^\infty F_{OPV}(\lambda)\varepsilon_{OPV}(\lambda)\lambda^4 d\lambda \tag{4.18}$$

$$\kappa^2 = (\cos\theta_T - 3\cos\theta_{OPV\#1}\cos\theta_{OPV\#2})^2 \tag{4.19}$$

The expression for κ^2 in a typical FRET experiment involves the orientation of the emission dipole moment of the donor ($\vec{\mu}_D$) with respect to the absorption dipole moment of the acceptor ($\vec{\mu}_A$) (see Figure 4.6). However, since the donor and acceptor are a same OPV molecule, whose absorption and emission dipole moments are parallel and oriented along the main axis of the OPV molecule, the expression for R_o, that would usually involve the energy donor (*D*) and acceptor (*A*), was modified to reflect this fact (OPV = *D* = *A*). In Equation 4.19, θ_T is the angle between the emission and absorption dipole moments, and θ_D and θ_A are the angles $\theta_{OPV\#1}$ and $\theta_{OPV\#2}$ between the emission or the absorption dipole moments of the OPV moieties located at each end of the complex and the vector joining them (Figure 4.6).[27]

To obtain the structure of (OPV-$Q_4A)_2$-Na, (OPV-$Q_8A)_2$-Na, and (OPV-$Q_{17}A)_2$-Na, the crystal structure of $(Q_8A)_2$-Na provided by Dr. Maurizot from the University of Bordeaux was imported in HyperChem. Four quinoline residues were removed at the end of each octamer to yield the $(Q_4A)_2$-Na complex, and nine quinoline residues were added at the end of each octamer to yield the $(Q_{17}A)_2$-Na complex. The OPVA moiety was added via a peptide bond at the *N*-terminal of the two foldamers constituting the (OPV-$Q_nA)_2$-Na complex, and its energy was minimized while keeping the complex unchanged in the molecular mechanics optimizations to yield the structure of the complexes (OPV-$Q_4A)_2$-Na, (OPV-$Q_8A)_2$-Na and (OPV-$Q_{17}A)_2$-Na shown in Figure 4.6.

The values of θ_T, θ_D, and θ_A for (OPV-$Q_4A)_2$-Na were found by HyperChem to equal 29, 94.5 and 85.5 ^{o}, respectively. Combining Equations 4.18 and 4.19 yielded a Förster Radius of 4.3

nm. However, since the distance between the centers of the two OPV moieties in (OPV-$Q_4A)_2$-Na was only 1.4 nm, less than half the value of R_o, strong FRET was expected to take place between the two OPV units in this metal complex, thus resulting in the instantaneous delocalization of the dipole moments and a lower r_o value as found in the TRFA measurements. In fact, the α value of 23 ^{o} found from r_o for the angle between $\vec{\mu}_A$ and $\vec{\mu}_D$ for the short complex agreed with the θ_T value of 29^o predicted from the (OPV-$Q_4A)_2$-Na structure shown in Figure 4.6. This conclusion further strengthens the notion that the small r_o value found for the short complex was a result of FRET occurring between the two OPV moieties. Applying the same protocol to (OPV-$Q_8A)_2$-Na, an R_o value of 3.2 nm and a separation distance of 3.0 nm between the centers of the two OPV units were obtained. In a similar way, the R_o value for (OPV-$Q_{17}A)_2$-Na was 1.15 nm and the distance separating donor from acceptor was 6.2 nm. Therefore, in these two latter cases, the two chromophores were separated by a long distance that was comparable to or much greater than R_o which resulted in weaker FRET and a r_o value that approached the r_o value expected for whole foldamers having a same number of units.

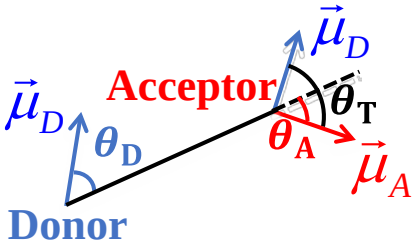

	$(OPV\text{-}Q_4A)_2$-Na	$(OPV\text{-}Q_8A)_2$-Na	$(OPV\text{-}Q_{17}A)_2$-Na
	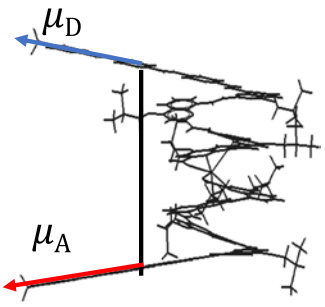	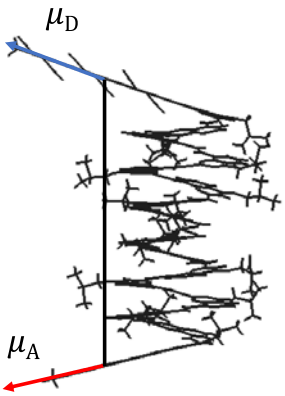	
θ_D	95°	116°	106°
θ_A	85°	64°	74°
θ_T	29 °	109°	81°
R_o (nm)	4.3	3.3	1.1
$d_{D\text{-}A}$(nm)	1.4	3.0	6.2
r_o	0.3	0.36	0.32
α	23°	15°	21°

Figure 4.6. Scheme representing the emission dipole moment of the donor ($\vec{\mu}_D$) and the absorption dipole moment of the acceptor ($\vec{\mu}_A$) and parameters retrieved from the optimized structures of $(OPV\text{-}Q_4A)_2$-Na, $(OPV\text{-}Q_8A)_2$-Na, and $(OPV\text{-}Q_{17}A)_2$-Na.

4.3.3 Rotational time of OPV-Q_8A-Na-Q_{16}A as a function of OPV-Q_8A concentration

The solution of OPV-Q_8A-Na-Q_{16}A, obtained by mixing 1.4×10^{-5} M OPV-Q_8A and 1.4×10^{-4} M Q_{16}A, was diluted in an effort to probe the equilibrium leading to foldamer complexation. OPV-Q_8A was first neutralized by NaOH to generate the carboxylate anion, that would induce its self-assembly with the carboxylate anion of another strand in apolar chloroform. Therefore, diluting the solution was expected to induce the dissociation of the OPV-Q_8A-Na-Q_{16}A complex into its shorter constituting elements, namely the OPV-Q_8A and Q_{16}A foldamers, which would result in shorter rotational times. In turn, analysis of the trends obtained by plotting the rotational time as a function of foldamer concentration should yield the equilibrium constant.

In the OPV-Q_8A-Na-Q_{16}A dilution test, the OPV-Q_8A:Q_{16}A molar ratio was kept constant and equal to 1:10, to favor the formation of the OPV-Q_8A-Na-Q_{16}A complex over that of the (OPV-Q_8A)$_2$-Na symmetric dimer. The three equilibria given in Equations 4.20 – 4.22 accounted for the five species present in solution, namely OPV-Q_8A, OPV-Q_8A-Na-Q_{16}A, (OPV-Q_8A)$_2$-Na, Q_{16}A, and (Q_{16}A)$_2$-Na. The same equilibrium constant (K) was used for the three equilibria. Equations 4.23 and 4.24 reflected the conservation of the species OPV-Q_8A and Q_{16}A in the solution based on their overall concentrations [OPV-Q_8A]$_o$ and [Q_{16}A]$_o$, respectively. Among the five species present in solution, the OPV-labeled macromolecules were solely detected in the TRFA experiments. Therefore, the number-average rotational time $<\phi>$ obtained from the mixture was expected to take the expression given in Equation 4.25 for the weighted average of the OPV-labeled unimers (r_{oU} = 0.37 and ϕ_{oU} = 0.78 ns for OPV-Q_8A), mixed foldamers (r_{oM} = 0.35 and ϕ_M = 1.69 ns for OPV-Q_8A-Na-Q_{16}A), and dimers (r_{oD} = 0.36 and ϕ_D = 1.24 ns for (OPV-Q_8A)$_2$-Na). Consequently, $<\phi>$ was expected to decrease from 1.7 ns for OPV-Q_8A-Na-Q_{16}A to 0.78 ns to OPV-Q_8A upon dilution of the solution.

$$2\ \text{OPV-Q}_8\text{A} \underset{}{\overset{K}{\rightleftharpoons}} (\text{OPV-Q}_8\text{A})_2\text{-Na} \tag{4.20A}$$

$$[(\text{OPV-Q}_8\text{A})_2\text{-Na}]=K\times[\text{OPV-Q}_8\text{A}]^2 \tag{4.20B}$$

$$\text{OPV-Q}_8\text{A}+\text{Q}_{16}\text{A} \underset{}{\overset{K}{\rightleftharpoons}} \text{OPV-Q}_8\text{A-Na-Q}_{16}\text{A} \tag{4.21A}$$

$$[\text{OPV-Q}_8\text{A-Na-Q}_{16}\text{A}]=K\times[\text{OPV-Q}_8\text{A}][\text{Q}_{16}\text{A}] \tag{4.21B}$$

$$2\ \text{Q}_{16}\text{A} \underset{}{\overset{K}{\rightleftharpoons}} (\text{Q}_{16}\text{A})_2\text{-Na} \tag{4.22A}$$

$$[(\text{OPV-Q}_{16}\text{A})_2\text{-Na}]=K\times[\text{OPV-Q}_{16}\text{A}]^2 \tag{4.22B}$$

$$[\text{OPV-Q}_8\text{A}]_o = [\text{OPV-Q}_8\text{A}] + [\text{OPV-Q}_8\text{A-Na-Q}_{16}\text{A}] + 2\times[(\text{OPV-Q}_8\text{A})_2] \tag{4.23}$$

$$[\text{Q}_{16}\text{A}]_o = [\text{Q}_{16}\text{A}] + [\text{OPV-Q}_8\text{A-Na-Q}_{16}\text{A}] + 2\times[(\text{Q}_{16}\text{A})_2\text{-Na}] \tag{4.24}$$

$$<\phi>=\frac{[\text{OPV-Q}_8\text{A}]\times r_{oU}\phi_U +[\text{OPV-Q}_8\text{A-Na-Q}_{16}\text{A}]\times r_{oM}\phi_M +2\times[(\text{OPV-Q}_8\text{A})_2\text{-Na}]\times r_{oD}\phi_D}{[\text{OPV-Q}_8\text{A}]\times r_{oU} +[\text{OPV-Q}_8\text{A-Na-Q}_{16}\text{A}]\times r_{oM} +2\times[(\text{OPV-Q}_8\text{A})_2\text{-Na}]\times r_{oD}} \tag{4.25}$$

The $I_{VV}(t)$, $I_{VH}(t)$, and $I_{VM}(t)$ decays were acquired for the 1:10 OPV-Q_8A:Q_{16}A mixtures as a function of concentration with a slit width for the emission monochromator that was set to 1 nm (instead of 12 nm in the fluorescence experiments presented thus far), to lower the rate of fluorescence counts to within 2.0 % of the 20 MHz repetition rate of the time-resolved fluorometer. Unfortunately, the 1 nm slit width generated a 100 ps contribution in all the fluorescence decays due to scattering of photons being clipped off by the monochromator slits. This contribution could

be handled mathematically by the analysis program *aniso01d* and did not affect the rotational times retrieved from the TRFA measurements. All the TRFA measurements presented fom this point on contained this 100 ps contribution. In the future, these decay aquisitions will be repeated with the wider 12 nm emission slits, used for the fluorescence measurements reported so far. The results of the dilution experiments are presented in Figure 4.7.

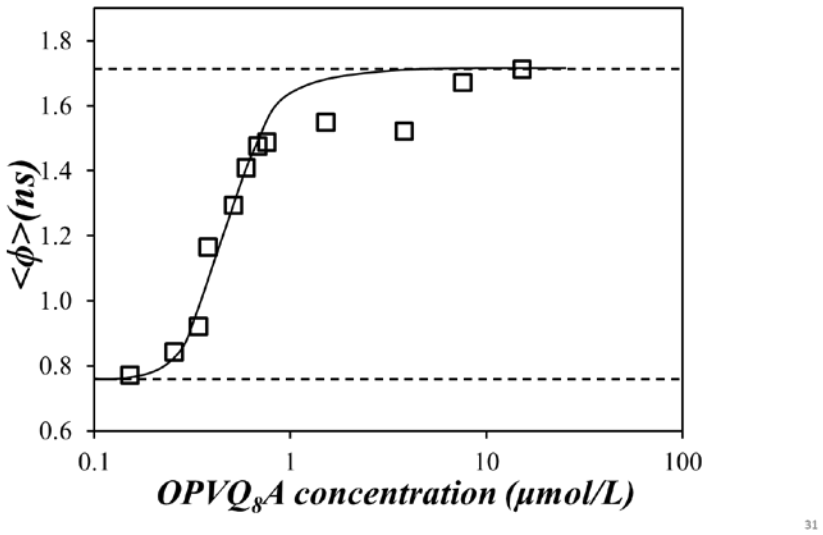

Figure 4.7. Rotation time of the 1:10 OPV-Q_8A:Q_{16}A mixture as a function of OPV-Q_8A concentration. Line is drawn to guide the eye.

The average rotational time plotted in Figure 4.7 increases with increasing foldamer concentration, from 0.75 ns at OPV-Q_8A concentrations below 0.1 μM to 1.7 ns at OPV-Q_8A concentrations greater than 6 μM. The rotational times of 0.75 and 1.7 ns were close to those of OPV-Q_8 and OPV-Q_{24} foldamers, respectively. The S-shape profile shown for the average rotational time of the 1:10 OPV-Q_8A:Q_{16}A mixture in Figure 4.7 is what would be expected from the dissociation of the OPV-Q_8A-Na-Q_{16}A complex into its two constituting elements.

A mathematical protocol was implemented whereby the concentration of the three species, OPV-Q_8A, $(OPV\text{-}Q_8A)_2$-Na, and OPV-Q_8A-Na-$Q_{16}A$, were calculated for a given *K* value and used to compare the $<\phi>$ values calculated from Equation 4.25 based on these concentrations and the $<\phi>$ values obtained experimentally in Figure 4.7. Unfortunately, poor agreement was obtained between the calculated and experimental $<\phi>$ values. This disagreement could have two causes. First, the same equilibrium constant (*K*) was employed to account for the three equilibria depicted in Equations 4.20 – 4.22. This assumption might be erroneous, as *K* might depend on foldamer length. This aspect of the dilution experiments will be investigated in the future. Second, the dilution experiments changed not only the foldamer concentration but also the ionic strength of the solution, since each foldamer was terminated by a carboxylate anion. Electrostatic repulsion at low foldamer concentration and screening effect at high foldamer concentration might complicate the analysis of the trend shown in Figure 4.7. Here again more experiments will be conducted in order to investigate the effect of ionic strength on these complexation experiments.

Despite the issues raised above, the most important result of the dilution study was the demonstration that the OPV-Q_8A-Na-$Q_{16}A$ complex dissociates upon dilution. These experiments imply that complexation, and thus foldamer elongation, can only take place above a threshold concentration.

4.3.4 Oligomerization of AQ_2PQ_2A monomers in the presence of an OPV-Q_8A stopper

The examples presented thus far of the metal complexation of two oligoquinolines terminated at one end with a carboxylate anion into a homo- ($(OPV\text{-}Q_8A)_2$-Na) or hetero- (OPV-Q_8A-Na-$Q_{16}A$) dimer are examples of closed association mechanisms. The main advantage of a closed association

mechanism resides in the formation of well-defined products, which can be more easily characterized. Its disadvantage in the context of foldamer elongation is that the dimensions of the final product are constrained by the size of the reactants. By contrast, an open association mechanism results in poorly defined products but offers the advantage of generating products with a broad size distribution, including a small fraction of products that could be theoretically of infinite size. With this in mind, the H-Lab in Bordeaux envisioned that a foldamer functionalized with a carboxylic acid at both termini could polymerize by undergoing metal complexation. To this end, the building block referred to as AQ_2PQ_2A was a pyridine flanked by two quinoline dimers and terminated at both ends with a carboxylic acid (see Figure 4.1). The oligomerization of AQ_2PQ_2A had already been identified by the H-Lab by using NMR, but the characterization of the oligomer size had remained elusive up to this point. Consequently, the complexation of AQ_2PQ_2A with itself and OPV-Q_8A as a fluorescent stopper was investigated, as it was expected to result in the formation of AQ_2PQ_2A oligomers ($(Q_2PQ_2)_n$) terminated with 0, 1, or 2 OPV-Q_8A units. In turn, TRFA measurements conducted on the OPV moiety located at the end of $(Q_2PQ_2)_n$ should yield their number-average rotational time $\langle\phi\rangle$, and thus their number average length.

Solutions containing a fixed 1.4×10^{-5} M concentration of OPV-Q_8A and different molar ratios of AQ_2PQ_2A:OPV-Q_8A were prepared. Their $I_{VV}(t)$ and $I_{VH}(t)$ decays were acquired and fitted with the program *aniso01d-4* by assuming a monoexponential TRFA (Equation 4.3). The rotational times retrieved from these experiments are shown in Figure 4.8.

Two types of AQ_2PQ_2A monomers were prepared in the H-Lab, depending on whether

isobutyl or hexyl side chains were employed to facilitate the solubilization of the resulting $(Q_2PQ_2)_n$ complexes. The hexyl side chain was found to provide better solubility than the isobutyl one. In both cases, ϕ increased with increasing AQ_2PQ_2A:OPV-Q_8A molar ratio before reaching a plateau at higher molar ratios. Based on the calibration curve established in Figure 3.5A, the plateau value reached by ϕ corresponded to that of an OPV-Q_n foldamer constituted of 24 or 30 units for the AQ_2PQ_2A monomer prepared with isobutyl or hexyl side chains, respectively. The traditional synthesis of Q_n foldamers with *n* equal to 24 or 30 would have been much more challenging to achieve by the traditional synthetic method, but further elongation of $(Q_2PQ_2)_n$ was prevented due to poor solubility.

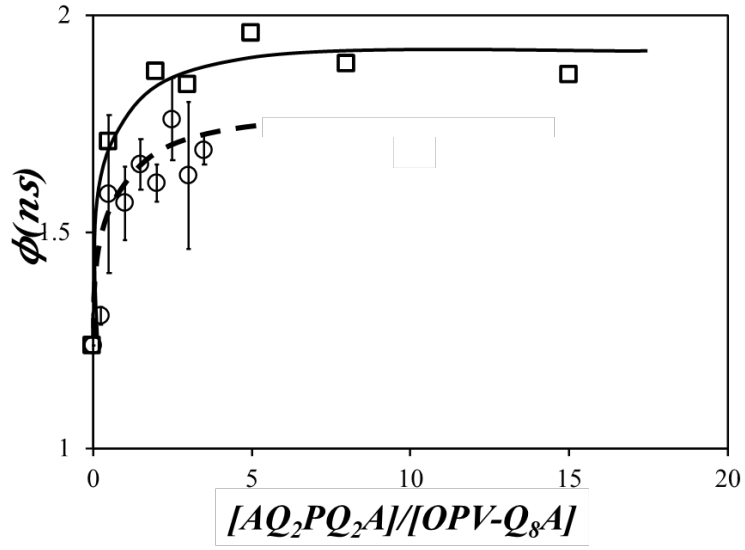

Figure 4.8. Plot of rotational time as a function of the AQ_2PQ_2A:OPV-Q_8A molar ratio obtained for mixtures of 1.4×10^{-5} M OPV-Q_8A and different amounts of AQ_2PQ_2A with (○, – –) isobutyl and (□, —) hexyl side chains.

The progressive increase in ϕ observed with increasing molar ratio in Figure 4.8 is a clear indication that oligomerization of AQ_2PQ_2A took place in solution, and that it could be evidenced by conducting TRFA measurements. Furthermore, the calibration curve established in Chapter 3 for the OPV-Q_n foldamers could be used to yield the size of the $(Q_2PQ_2)_n$ oligomers based on the size of an equivalent OPV-Q_n foldamer. In conclusion, this study demonstrates the potential of this metal complexation procedure for foldamer elongation.

4.4 Conclusions

It was demonstrated in this chapter that TRFA is a convincing method to characterize the size of products obtained by the self-assembly of foldamer acids induced by metal coordination. The calibration curve determined in Chapter 3 was used to establish that the rotational time of a metal complex was the same as that of an OPV-Q_n oligomer with a number of units *n* equal to the sum of the number of units of the two foldamers constituting the complex. This result demonstrated that a foldamer complex remained a rigid object in solution. In turn, metal coordination opens a new venue to generate well-defined OPV-Q_n foldamers with an *n* value as large as 66. This conclusion was reached by taking advantage of the ability of our analysis programs to isolate the wobbling of the OPV dye from the tumbling of the foldamers with a number of units larger than 41.

The dilution experiments conducted with the OPV-Q_8A-Na-$Q_{16}A$ complexes demonstrated that these complexes were the result of an equilibrium and that lowering the concentrations of the constituting foldamers resulted in the dissociation of the complexes. This equilibrium was taken advantage of to induce the oligomerization of two AQ_2PQ_2A building blocks whose average size

could be determined by TRFA measurements.

In conclusion, Chapter 4 demonstrated that the self-assembly of foldamer acids by metal coordination represents a viable procedure to elongate foldamers according to a closed or an open association mechanism. The size of the foldamer complexes generated in the process can be estimated by applying TRFA.

Chapter 5

Conclusions and future work

This study represented the first example in the scientific literature where TRFA was applied to characterize the size of whole or complexed foldamers in solution. Over the course of this project, a series of quinoline-based foldamers, terminated by either ester (Q_n) or carboxylic acid (Q_nA) groups, were successfully prepared and selectively labeled with OPV as a dye to form OPV-Q_nA or OPV-Q_n in the H-Lab or by myself.

Solutions of OPV-Q_n in chloroform were excited with vertically polarized light, and the $I_{VV}(t)$ and $I_{VH}(t)$ fluorescence decays were acquired by monitoring the fluorescence intensity vertically or horizontally polarized, respectively. The decays were globally analyzed by assuming a monoexponential TRFA equation to yield the rotational time of the OPV-Q_n foldamers. The rotational time was found to increase linearly with increasing foldamer length, which demonstrated that the hydrodynamic volume of the OPV-Q_n foldamer was increased by a set amount upon addition of one quinoline unit to the foldamer. Furthermore, the hydrodynamic volume of the OPV-Q_n foldamers in solution agreed perfectly with their dimensions expected from SCXRD analysis. This study established the reliability of TRFA to probe the structure of rigid helical foldamers in solution.

Following these preliminary TRFA experiments, the linear relationship found between rotational time and oligomer chain length was used as a calibration curve to determine the size of the self-assembled foldamers prepared by metal complexation. Comparison of the rotational times obtained for the complexes with this calibration curve indicated that the complexation of foldamers Q_nA and Q_mA with one sodium ion resulted in the formation of an extended foldamer with a NU value equal to the sum of the NU values of its constituting parts (i.e. n + m). This result suggested

that the foldamer complex remained rigid after self-assembly of the constituting foldamers induced by metal coordination. Consequently, this study demonstrated that the complexation of foldamers by metal coordination provides a novel experimental means to elongate foldamer strands into rigid folded complexes that is much easier and faster than traditional elongation methods based on synthesis.

The dilution test conducted for the OPV-Q_8A-Na-Q_{16}A indicated that complex formation between two foldamers is based on an equilibrium and is driven by foldamer concentration. Addition of increasing amounts of AQ_2PQ_2A to an OPV-Q_8A solution induced the formation of oligomeric compounds whose average chain length was determined by TRFA measurements. Unfortunately, extension of the oligomers was limited by their poor solubility. The solubility issue will need to be resolved in the future to prepare longer foldamers.

In summary, the TRFA offers an experimental means to characterize the size and dynamics of oligoquinoline-based foldamers labeled with OPV in solution.

In terms of future work, the experiments described in this thesis have open a new means to probe foldamers in solution. A lot still remains to be done. First, the dilution test conducted with the OPV-Q_8A-Na-Q_{16}A complexes needs to be repeated using 12 instead of 1 nm slit width for the emission monochromator to avoid the 100 ps artefact in the $I_{VV}(t)$ and $I_{VH}(t)$ decays. The binding constant for the equilibrium describing the formation of the foldamer complexes needs to be determined. Current derivations fail to properly describe the trends obtained when plotting $<\phi>$ as a function of foldamer concentration. A study of electrostatic effects, that might affect the equilibrium between these charged foldamers, must be conducted. Also, the foldamer size might affect the association mechanism. The possible dependency of the binding constant on foldamer length needs to be resolved to better understand the oligomerization of the AQ_2PQ_2A monomers.

More work needs to be carried for the oligomerization experiments that would cover a wider range of monomer concentration as compared to what has been accomplished so far in Figure 4.8.

References

(1) Gellman, S. H. Foldamers: A Manifesto. *Acc.Chem. res.* **1998**, *31*,173-180

(2) Guichard, G.; Huc, I. Synthetic Foldamers. *Chem. Commun.* **2011**, *47*, 5933–5941.

(3) Cole, J. P.; Hanlon, A. M.; Rodriguez, K. J.; Berda, E. B. Protein-like Structure and Activity in Synthetic Polymers. *J. Polym. Sci. Part A Polym. Chem.* **2017**, *55* , 191–206.

(4) Goodman, C. M.; Choi, S.; Shandler, S.; DeGrado, W. F. Foldamers as Versatile Frameworks for the Design and Evolution of Function. *Nat. Chem. Biol.* **2007**, *3*, 252–262.

(5) Hecht, S.; Huc, I. *Foldamers : Structure, Properties, and Applications*; Wiley-VCH, 2007.

(6) Wolffs, M.; Delsuc, N.; Veldman, D.; Anh, N. V.; Williams, R. M.; Meskers, S. C. J.; Janssen, R. A. J.; Huc, I.; Schenning, A. P. H. J. Helical Aromatic Oligoamide Foldamers as Organizational Scaffolds for Photoinduced Charge Transfer. *J. Am. Chem. Soc.* **2009**, *131*, 4819–4829.

(7) Li, X.; Markandeya, N.; Jonusauskas, G.; McClenaghan, N. D.; Maurizot, V.; Denisov, S. A.; Huc, I. Photoinduced Electron Transfer and Hole Migration in Nanosized Helical Aromatic Oligoamide Foldamers. *J. Am. Chem. Soc.* **2016**, *138*, 13568–13578.

(8) Carini, M.; Ruiz, M. P.; Usabiaga, I.; Fernández, J. A.; Cocinero, E. J.; Melle-Franco, M.; Diez-Perez, I.; Mateo-Alonso, A. High Conductance Values in π-Folded Molecular Junctions. *Nat. Commun.* **2017**, *8*, 15195.

(9) Yu, Z.; Hecht, S. Cooperative Switching Events in Azobenzene Foldamer Denaturation. *Chem. - A Eur. J.* **2012**, *18*, 10519–10524.

(10) Li, X.; Qi, T.; Srinivas, K.; Massip, S.; Maurizot, V.; Huc, I. Synthesis and Multibromination of Nanosized Helical Aromatic Amide Foldamers via Segment-Doubling Condensation. *Org. Lett.* **2016**, *18*, 1044–1047.

(11) Wang, X.; Wicher, B.; Ferrand, Y.; Huc, I. Orchestrating Directional Molecular Motions: Kinetically Controlled Supramolecular Pathways of a Helical Host on Rodlike Guests. *J. Am. Chem. Soc.* **2017**, *139*, 9350–9358.

(12) Jiang, H.; Léger, J.-M.; Huc, I. Aromatic δ-Peptides. *J. Am.Chem.Soc*. **2003**, 125, 3448-3449.

(13) Zhang, D.-W.; Zhao, X.; Hou, J.-L.; Li, Z.-T. Aromatic Amide Foldamers: Structures, Properties, and Functions. *Chem. Rev.* **2012**, *112*, 5271–5316.

(14) Cheong, C.; Varani, G.; Tinoco, I. Solution Structure of an Unusually Stable RNA Hairpin, 5GGAC(UUCG)GUCC. *Nature* **1990**, *346*, 680–682.

(15) Holbrook, S. R.; Cheong, C.; Tinoco, I.; Kim, S.-H. Crystal Structure of an RNA Double Helix Incorporating a Track of Non-Watson–Crick Base Pairs. *Nature* **1991**, *353*, 579–581.

(16) Kanyo, J. E.; Duhamel, J.; Lu, P. Secondary Structure of the r(CUUCGG) Tetraloop. *Nucleic Acids Res.* **1996**, *24*, 4015–4022.

(17) Soptokova-de Olivera Santos,J.; Voisin-Chiret, A.S.; Burzicki,G.; Sebaoun, L.; Sebban, M.; Lohier, J.-F.; Legay, R.; Oulyadi, H.; Bureau, R.; Rault, S. Structural Characterizations of Oligopyridyl Foldamers, α-Helix Mimetics. *J. Chem.Inf, Model.* **2012**, 52, 429-439.

(18) Hartley, C. S. Folding of *Ortho* -Phenylenes. *Acc. Chem. Res.* **2016**, *49*, 646–654.

(19) Kirshenbaum, K.; Barron, A. E.; Goldsmith, R. A.; Armand, P.; Bradley, E. K.; Truong, K. T.; Dill, K. A.; Cohen, F. E.; Zuckermann, R. N. Sequence-Specific Polypeptoids: A Diverse Family of Heteropolymers with Stable Secondary Structure. *Proc. Natl. Acad. Sci. U. S. A.* **1998**, *95*, 4303–4308.

(20) Hua, Y.; Flood, A. H. Flipping the Switch on Chloride Concentrations with a Light-Active Foldamer. *J. Am. Chem. Soc.* **2010**, *132* , 12838–12840.

(21) Buffeteau, T.; Ducasse, L.; Poniman, L.; Delsuc, N.; Huc, I. Vibrational Circular Dichroism and Ab Initio Structure Elucidation of an Aromatic Foldamer. *Chem. Commun.* **2006**, *25*, 2714-2716.

(22) Bornhof, A.-B.; Bauzá, A.; Aster, A.; Pupier, M.; Frontera, A.; Vauthey, E.; Sakai, N.; Matile, S. Synergistic Anion–$(\pi)_n$ –π Catalysis on π-Stacked Foldamers. *J. Am. Chem. Soc.* **2018**, *140*, 4884–4892.

(23) Berne, B. J.; Pecora, R. *Dynamic Light Scattering with Applications to Chemistry, Biology, and Physics*; Dover Publications: Mineola,NY,2000.

(24) Kelley, R. F.; Rybtchinski, B.; Stone, M. T.; Moore, J. S.; Wasielewski, M. R. Solution-Phase Structure of an Artificial Foldamer: X-Ray Scattering Study. *J. Am. Chem. Soc.* **2007**,129, 4114-4115.

(25) Duhamel, J.; Kanyo, J.; Dinter-Gottlieb, G.; Lu, P.; Fluorescence Emission of Ethidium Bromide Intercalated in Defined DNA Duplexes: Evaluation of Hydrodynamics Components. *Biochemistry* **1996**, *35*,16687-16697.

(26) Qi, T.; Deschrijver, T.; Huc, I. Large-Scale and Chromatography-Free Synthesis of an Octameric Quinoline-Based Aromatic Amide Helical Foldamer. *Nat. Protoc.* **2013**, *8*, 693–708.

(27) Lakowicz, J. R. *Principles of Fluorescence Spectroscopy* 2nd Ed., Kluwer Acad. New York, **1999**.

(28) Berlman, I. B, *Handbook of Fluorescence Spectra of Aromatic Molecules*.; Academic Press: New York, 1965

(29) *CRC Handbook of Chemistry and Physics, 84th* Ed.; CRA Press: Boca Raton, FL, 2003.

(30) Egelhaaf, H.-J.; Lüer, L.; Tompert, A.; Bäuerle, P.; Müllen, K.; Oelkrug, D. Fluorescence Anisotropy and Rotational Diffusion of Polyene-like Molecules in Solution. *Synth. Met.* **2000**, *115*,

63–68.

(31) Schäfer, J.; Breul, A.; Birckner, E.; Hager, M. D.; Schubert, U. S.; Popp, J.; Dietzek, B. Fluorescence Study of Energy Transfer in PMMA Polymers with Pendant Oligo-Phenylene-Ethynylenes. *ChemPhysChem* **2013**, *14*, 170–178.

(32) Chuang, T. J.; Eisenthal, K. B. Theory of Fluorescence Depolarization by Anisotropic Rotational Diffusion. *J. Chem. Phys.* **1972**, *57*, 5094–5097.

(33) Tirado, M. M.; de la Torre, J. G. Rotational Dynamics of Rigid, Symmetric Top Macromolecules. Application to Circular Cylinders. *J. Chem. Phys.* **1980**, *73*, 1986–1993.

(34) Fujimoto, B. S.; Miller, J. M.; Ribeiro, N. S.; Schurr, J. M. Effects of Different Cations on the Hydrodynamic Radius of DNA. *Biophys. J.* **1994**, *67*, 304–308.

(35) Duhamel, J. Global Analysis of Fluorescence Decays to Probe the Internal Dynamics of Fluorescently Labeled Macromolecules. *Langmuir* **2014**, *30*, 2307–2324.

(36) Hennecke, M.; Damerau, T.; Muellen, K. Fluorescence Depolarization in Poly(p-Phenylphenylenevinylene) and Related Oligomers. *Macromolecules* **1993**, *26*, 3411–3418.

(37) Wang, J.; Little, H.; Duhamel, J.; Li, X.; Markandeya, N.; Maurizot, V.; Huc, I. Application of Time-Resolved Fluorescence Anisotropy to Probe Quinoline-Based Foldamers Labeled with Oligo(phenylene vinylene). *Macromolecules* **2019**, 52, 5829-5837.

Appendices

A] ^{1}H-NMR (300MHz, $CHCl_3$)

OPV-Q_7E

^{1}H NMR ($CDCl_3$, 300 MHz) δ (ppm): 11.59 (s, 1H), 11.47 (s, 1H), 11.40 (s, 1H), 11.21 (s, 1H), 11.05 (s, 1H), 11.01 (s, 1H), 10.99 (s, 1H), 8.27 (d, *J =7.5 Hz*, 1H), 8.21-8.14 (m, 3H), 8.10 (d, *J =7.5 Hz*, 1H), 7.99-7.88(m, 4H), 7.86 (d, *J =7.8 Hz*, 1H), 7.84-7.76 (m, 3H), 7.54 (s, 2H), 7.52-7.30 (m), 7.23-7.14 (m, 3H), 7.11-7.01 (m, 2H), 6.93 (s, 1H), 6.88 (s, 1H), 6.87 (s, 1H), 6.81 (s, 1H), 6.77 (s, 1H), 6.71 (s, 1H), 6.65 (s, 1H), 6.60 (s, 1H), 6.44 (s, 1H), 5.92 (s, 1H), 4.26-4.15 (m, 3H), 4.11-4.01 (m, 2H) 4.01-3.87 (m, 9H), 3.84 (s, 2H), 3.81 (s, 2H), 3.80-3.70 (m, 5H), 3.68-3.57 (m, 2H), 3.08 (s, 3H), 2.64-2.12 (m, 14H), 2.32 (s, 3H), 1.95 (sept, 1H), 1.69 (s, 3H), 1.44-1.35 (m, 13H), 1.34-1.10 (m, 55H), 1.02 (d, *J =6.6 Hz*, 3H), 0.88 (d, *J =6.6 Hz*, 3H), 0.84-0.74 (m, 6H). 0.02 (d, *J =6.6 Hz*, 3H), -0.05 (d, *J =6.6 Hz*, 3H); HRMS (ES^+): m/z calculated for $C_{147}H_{168}O_{22}N_{14}$ $[M+2H]^{2+}$: 1242.1318; Found: 1242.13057

Q_8A

^{1}H NMR($CDCl_3$, 300 MHz): δ 11.30 (s, 1H), 11.18 (s, 1H), 11.08 (s, 1H), 11.01 (s, 1H), 10.98 (s, 1H), 10.96 (s, 1H), 10.83 (s, 1H), 8.32 (dd, J = 8.3, 1.5 Hz, 1H), 8.23 (dd, J =7.7, 1.2 Hz, 2H), 8.18 (dd, J = 4.2, 1.3 Hz, 1H), 8.16 (dd, J = 3.6, 1.3 Hz, 1H), 8.12 (dd, J =8.3, 1.3 Hz, 1H), 8.05 (dd, J = 7.7, 1.2 Hz, 1H), 7.91 (dd, J = 3.0, 1.3 Hz, 1H), 7.90 – 7.85 (m,2H), 7.84 (s, 1H), 7.81 (s, 1H), 7.66 (dd, J = 7.7, 1.3 Hz, 1H), 7.54 (dd, J = 7.6, 1.2 Hz, 1H),7.44 (td, J = 8.0, 4.2 Hz, 2H), 7.35 – 7.21 (m, 6H), 7.19 – 7.12 (m, 1H), 7.06 (s, 1H), 7.02(s,1H), 6.98 (d, J = 8.0 Hz, 1H), 6.80 (s, 1H), 6.69 (s, 1H), 6.52 (s, 1H), 6.48 (s, 1H), 6.45 (s, 1H),6.15 (s, 1H), 4.18 – 4.04 (m, 3H), 4.04 – 3.81 (m, 10H), 3.74 (d, J = 6.4 Hz, 2H), 3.66 (dd, J =9.1, 7.4 Hz, 1H), 2.51 (m, 2H), 2.44 – 2.25 (m,5H), 2.25 – 2.18 (m, 1H), 1.38 – 1.33 (m, 8H),1.27 – 1.10 (m, 40H). MS (ES^+): m/z calculated for $C_{112}H_{112}N_{16}O_{19}$ $[M+H]^+$ 1986.8 found 1986.8.

$Q_{16}A$

^{1}H NMR(CDCl3, 300 MHz): δ10.93 (s, 1H), 10.73 (s, 2H), 10.56 (s, 1H), 10.54 (s, 1H), 10.38 (s, 1H), 10.36 (s, 1H),10.24 (s, 1H), 10.22 (s, 1H), 10.17 – 9.94 (m, 6H), 8.21 (dd, J = 8.1, 1.5 Hz, 1H), 8.08 – 7.98(m, 2H), 7.91 (dd, J = 7.3, 0.9 Hz, 1H), 7.88 – 7.57 (m, 15H), 7.28 – 6.74 (m, 31H), 6.59 (s,1H), 6.49 (s, 1H), 6.36 (s, 1H), 6.16 (s, 1H), 6.13 (s, 1H), 5.97 – 5.88 (m, 3H), 5.85 – 5.76 (m,5H), 5.75 (s, 1H), 4.01 – 3.48 (m, 32H), 2.45 – 2.10 (m, 16H), 1.42 – 0.95 (m, 96H). MS (ES$^+$):m/z calculated for $C_{224}H_{224}N_{32}O_{35}$ $[M]^+$ 3924.68 found 3924.69.

OPV-$Q_{17}E$

^{1}H NMR ($CDCl_3$, 300 MHz) δ ppm = 11.10 (1H, s), 11.05 (1H, s), 10.81 (1H, s), 10.52 (1H, s), 10.47 (1H, s), 10.37 (1H, s), 10.27 (1H, s), 10.20 (1H, s), 10.15 (1H, s), 10.11 (1H, s), 10.01 (1H, s), 9.98 (1H, s), 9.96 (1H, s), 9.92 (1H, s), 9.87 (3H, s), 7.93 (1H, d, J = 7.40 Hz), 7.86 (1H, d, J = 7.35 Hz), 7.77 (2H, d, J = 7.91 Hz), 7.72 (3H, d, J = 7.99 Hz), 7.49-7.69 (14H, m), 7.43 (3H, s), 7.06-7.23 (7H, m), 6.69-7.06 (28H, m), 6.65 (1H, s), 6.55 (2H, d, J = 9.88 Hz), 6.38 (2H, d, J = 9.28 Hz), 6.20 (1H, s), 6.13 (2H, d, J = 5.68 Hz), 5.90 (2H, d, J = 4.87 Hz), 5.61-5.78 (9H, m), 3.80-3.96 (5H, m), 3.43-3.79 (41H, m), 2.82 (3H, s), 1.93-2.38 (26H, m), 0.27-1.26 (120H, m), 0.85 (3H, d, J = 6.67 Hz), 0.71(3H, d, J = 6.67 Hz), 0.64 (3H, d, J = 6.67 Hz), 0.60 (3H, d, J = 6.67 Hz), -0.25 (3H, d, J = 6.48 Hz), -0.31 (3H, d, J = 6.70 Hz). HRMS (ESI$^+$): *m/z* calculated for $C_{287}H_{310}N_{34}O_{42}$ $[M+2H]^{2+}$: 2453.6634; found 2453.6588.

OPV-$Q_{24}E$

^{1}H NMR ($CDCl_3$, 300 MHz) δ (ppm): 11.102 (s, 1H), 11.057 (s, 1H), 10.531 (s, 1H), 10.471 (s, 1H), 10.364 (s, 1H), 10.252 (s, 1H), 10.172 (s, 1H), 10.132 (s, 1H), 10.084 (s, 1H), 9.970 (s, 1H), 9.926 (s, 1H), 9.890 (s, 1H), 9.839 (s, 1H), 9.780 (s, 1H), 9.738 (s, 1H), 9.728 (s, 1H), 9.710-9.578 (m, 8H), 7.946 (d, *J =7.5 Hz*, 1H), 7.883 (d, *J =7.5 Hz*, 1H), 7.803-7.416 (m, 28H), 7.299-7.022

(m, 10H), 7.022-6.715 (m, 28H), 6.715-6.559 (m, 12H), 6.542 (s, 1H), 6.408 (s, 1H), 6.382 (s, 1H), 6.220 (s, 1H), 6.146 (s, 1H), 6.116 (s, 1H), 5.896 (s, 1H), 5.887 (s, 1H), 5.738 (s, 1H), 5.726 (s, 1H), 5.707(s, 1H), 5.687 (s, 1H), 5.674-5.629 (m, 2H) 5.629-5.576 (m, 4H) 5.576-5.509 (m, 5H) 3.985-3.826 (m, 5H), 3.826-3.492 (m, 39H),3.492-3.316 (m, 13H), 2.8372 (s 3H), 2.405-1.926 (m, 31H), 1.865-1.750 (m,3H), 1.288-0.934 (m, 158H), 0.934-0.868 (m, 5H), 0.726 (d, *J =6.7 Hz*, 3H), 0.6653(d, *J =6.7 Hz*, 3H), 0.6314(d, *J =6.7 Hz*, 3H), -0.2387(d, *J =6.7 Hz*, 3H), -0.2979(d, *J =6.7 Hz*, 3H). HRMS (ES^+): m/z calculated for $C_{385}H_{406}O_{56}N_{48}$ $[M+2H]^{2+}$: 2201.3583; Found: 2201.37726

B] Time-Resolved Fluorescence Decay Analysis:

As discussed in the Experimental section of Chapter 3, the standard procedure applied to determine the time-resolved fluorescence anisotropy (TRFA = $r(t)$) is by acquiring the $I_{VV}(t)$ and $I_{VH}(t)$ fluorescence decays simultaneously by continuously alternating the orientation of the emission polarizer and acquiring the fluorescence signal for short durations at the time. This procedure accounts for fluctuations in the intensity of the excitation source which would affect the overall fluorescence intensity of the $I_{VV}(t)$ and $I_{VH}(t)$ decays over the decay acquisition time. The decays are then combined into Equation B1 to yield the TRFA. Since fluctuations in the intensity of the excitation source are accounted for, the *G*-factor handles the difference in the detection efficiency of the instrument between the two orientations of the emission polarizer and needs to be determined independently.

$$r(t) = \frac{I_{VV}(t) - G \times I_{VH}(t)}{I_{VV}(t) + 2G \times I_{VH}(t)} \qquad \text{(B1)}$$

Yet the expression of $r(t)$ in Equation B1 is derived from Equations 3.1 and 3.2 in the main text where *G* is a simple scaling factor which can be optimized through global analysis of the $I_{VV}(t)$ and $I_{VH}(t)$ fluorescence decays. This procedure was successfully implemented in 2004[1] for the global analysis of the monomer and excimer fluorescence decays of pyrene-labeled macromolecules in solution and its efficacy in fluorescence decay analysis has led to the publication of a number of reviews.[2,3] The same logic was applied to the global analysis with Equations 3.1 and 3.2 of the $I_{VV}(t)$ and $I_{VH}(t)$ fluorescence decays acquired with the OPV-Q_n constructs studied in this report.

Acknowledging that the procedure applied to globally analyze the polarized fluorescence decays according to Equations 3.1 and 3.2 might appear somewhat unorthodox, the parameters retrieved from the analysis of the fluorescence decays acquired with the 9 foldamers and listed in Tables D1 and D2 in Appendix D were utilized to generate 20 $I_{VV}(t)$ and 20 $I_{VH}(t)$ fluorescence decays for each foldamer using Equations 3.1 and 3.2, respectively. The decays were convoluted to the experimental instrument response function (IRF) and different patterns of Poisson noise were added, thus generating a grand total of 360 decays. The analysis of the decays was then conducted globally with the program aniso01c and the r_o and ϕ parameters obtained from the analysis of the experimental and simulated fluorescence decays were compared in Figure B1.

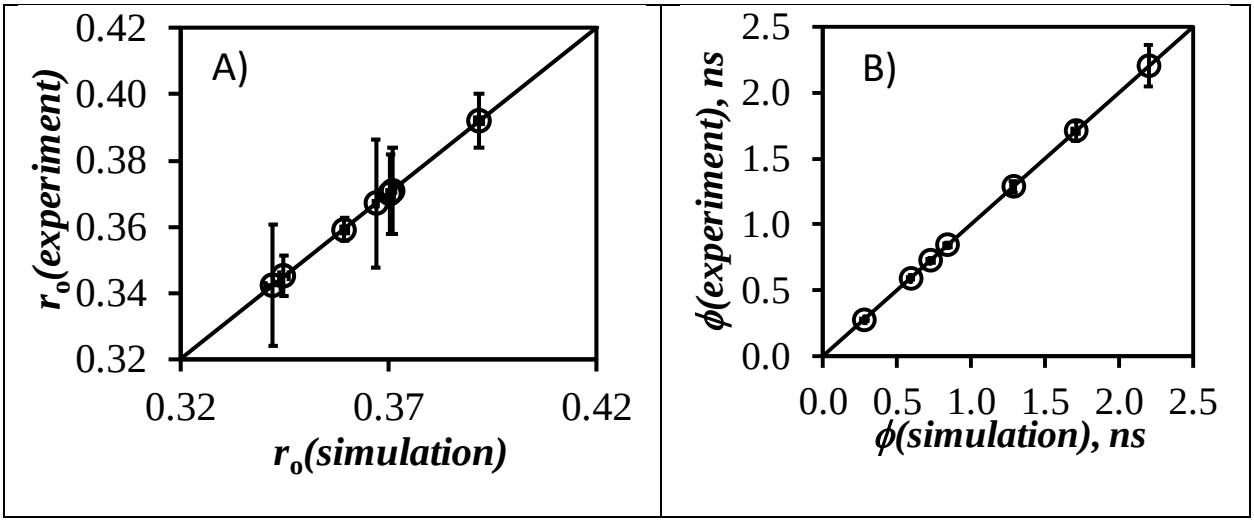

Figure B1. Comparison of the parameters A) r_o and B) ϕ retrieved from the global analysis of the experimental and simulated fluorescence decays.

The r_o and ϕ parameters were found to cluster perfectly along the diagonals in Figure B1 indicating that the program retrieved accurately these parameters. Furthermore, the error on the parameters retrieved from the analysis of the simulated fluorescence decays was minuscule compared to that

obtained from the analysis of the experimental fluorescence decays. This observation confirmed that experimental errors, most probably due to the instrument and sample solubility, dwarfed those generated by the analysis program. The excellent agreement found in Figure B1 between the analysis of the simulated and experimental decays validated the procedure applied in this study to analyze the polarized fluorescence decays of the OPV-Q_n constructs. A follow up study will provide further evidence of the robustness of this new experimental procedure and will be submitted shortly.

C] Dilution study of OPV-Q_{33}.

The rotational time of OPV-Q_{33} was monitored as a function of foldamer concentration. As can be seen in Figure C1, ϕ remained constant with foldamer concentration indicating that these molecules were not aggregated in chloroform.

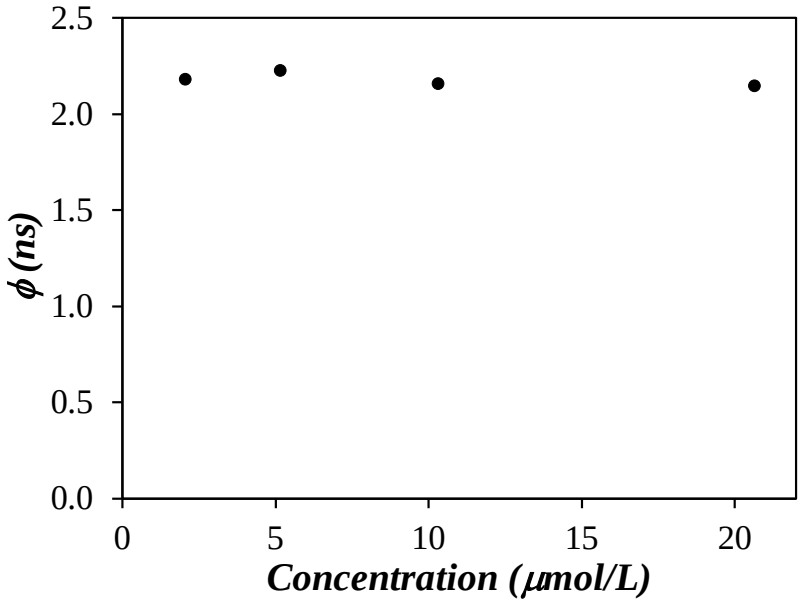

Figure C1. Plot of ϕ as a function of OPV-Q_{33} concentration in chloroform.

D] Parameters obtained from the fluorescence decay analysis.

Table D1. Parameters retrieved from the analysis of the $I_{VV}(t)$ and $I_{VH}(t)$ decays acquired with 10,000 counts at the decay maximum fitted globally when the anisotropy is a monoexponential (aniso01c) and with the triexponential given in Equation 3.19 (aniso02n-3).

	aniso01c				aniso02n-3					
Sample	r_0	ϕ (ns)	τ_o (ns)	χ^2	$D_{//}$ (ns^{-1})	$D_{\perp}$ (ns^{-1})	r_0	$<\phi>$ (ns)	τ_o (ns)	χ^2
OPV-Q_4	0.382	0.578	1.67	1.28	0.285	0.285	0.387	0.586	1.67	1.27
	0.377	0.573	1.64	1.24	0.273	0.316	0.375	0.569	1.64	1.25
	0.362	0.596	1.68	1.21	0.283	0.283	0.362	0.586	1.69	1.20
OPV-Q_7	0.356	0.727	1.59	1.09	0.223	0.240	0.356	0.721	1.59	1.08
	0.386	0.735	1.59	1.16	0.230	0.230	0.387	0.725	1.60	1.13
	0.367	0.709	1.59	1.23	0.137	0.378	0.383	0.729	1.59	1.22
OPV-Q_9	0.386	0.861	1.58	1.19	0.132	0.289	0.395	0.848	1.59	1.15
	0.351	0.866	1.59	1.17	0.194	0.194	0.349	0.861	1.59	1.17
	0.354	0.831	1.57	1.15	0.204	0.204	0.350	0.818	1.58	1.14
OPV-Q_{17}	0.357	1.214	1.59	1.14	0.097	0.175	0.363	1.273	1.58	1.13
	0.360	1.282	1.58	1.22	0.116	0.154	0.357	1.249	1.58	1.22
	0.362	1.315	1.57	1.30	0.132	0.132	0.356	1.264	1.59	1.22
OPV-Q_{24}	0.346	1.857	1.61	1.21	0.148	0.052	0.345	1.745	1.62	1.17
	0.339	1.597	1.59	1.21	0.075	0.134	0.345	1.667	1.59	1.20
	0.350	1.774	1.58	1.19	0.075	0.131	0.344	1.679	1.59	1.16
OPV-Q_{33}	0.344	2.303	1.59	1.28	0.062	0.108	0.323	2.028	1.61	1.28
	0.325	2.083	1.60	1.16	0.037	0.124	0.339	2.368	1.59	1.16
	0.313	2.013	1.61	1.16	0.041	0.119	0.333	2.382	1.60	1.12
OPVA	0.394	0.268	1.72	1.08						
	0.383	0.284	1.73	1.12						
	0.399	0.275	1.72	1.04						

Table D2. Parameters retrieved from the analysis of the $I_{VV}(t)$ and $I_{VH}(t)$ decays of foldamer ester acquired with 20,000 counts at the decay maximum fitted globally when the anisotropy is a monoexponential (aniso01c) and with the triexponential given in Equation 3.19 (aniso02n-3).

	aniso01c				aniso02n-3					
Sample	r_0	ϕ (ns)	τ_o (ns)	χ^2	$D_{//}$ (ns^{-1})	$D_{\perp}$ (ns^{-1})	r_0	$<\phi>$ (ns)	τ_o (ns)	χ^2
OPV-Q_4	0.360	0.606	1.69	1.16	0.276	0.276	0.360	0.605	1.69	1.15
	0.357	0.596	1.64	1.25	0.257	0.314	0.358	0.587	1.65	1.22
	0.376	0.596	1.67	1.25	0.203	0.387	0.390	0.593	1.67	1.18
OPV-Q_7	0.367	0.715	1.59	1.29	0.178	0.314	0.373	0.704	1.60	1.24
	0.382	0.731	1.59	1.16	0.230	0.230	0.382	0.723	1.60	1.14
	0.353	0.730	1.59	1.23	0.164	0.358	0.358	0.737	1.59	1.24
OPV-Q_9	0.396	0.824	1.58	1.29	0.122	0.325	0.392	0.834	1.59	1.17
	0.356	0.827	1.60	1.20	0.343	0.086	0.836	0.836	1.60	1.20
	0.352	0.837	1.58	1.20	0.251	0.154	0.355	0.831	1.58	1.20
OPV-Q_{17}	0.354	1.241	1.59	1.20	0.077	0.195	0.366	1.350	1.58	1.18
	0.364	1.366	1.57	1.28	0.119	0.155	0.358	1.228	1.59	1.19
	0.359	1.312	1.58	1.16	0.092	0.171	0.357	1.324	1.58	1.17
OPV-Q_{24}	0.335	1.684	1.59	1.28	0.996	0.100	0.335	1.673	1.59	1.28
	0.343	1.692	1.62	1.26	0.179	0.034	0.242	1.721	1.62	1.22
	0.339	1.626	1.60	1.21	0.061	0.136	0.347	1.816	1.60	1.03
OPV-Q_{33}	0.321	2.023	1.61	1.11	0.039	0.117	0.342	2.447	1.60	1.08
	0.337	2.360	1.59	1.43	0.035	0.115	0.341	2.611	1.60	1.30
	0.329	2.354	1.60	1.22	0.035	0.120	0.347	2.547	1.60	1.13

Table D3. Parameters of OPV-Q_nA retrieved from the analysis of the $I_{VV}(t)$ and $I_{VH}(t)$ decays acquired with 20,000 counts at the decay maximum fitted globally when the anisotropy is a monoexponential (aniso01c) and with the triexponential given in Equation 3.19 (aniso02n-3).

	aniso01d-4				aniso02n-3				
Sample	r_0	ϕ (ns)	τ_o (ns)	χ^2	$D_{//}$ (ns^{-1})	$D_{\perp}$ (ns^{-1})	r_0	τ_o (ns)	χ^2
OPV-Q_4A	0.341	0.621	1.690	1.262	0.268	0.268	0.341	1.691	1.260
	0.308	0.630	1.699	1.279	0.316	0.217	0.310	1.701	1.277
OPV-Q_8A	0.341	0.809	1.608	1.238	0.206	0.206	0.341	1.609	1.219
	0.323	0.781	1.617	1.256	0.343	0.100	0.333	1.610	1.291
	0.359	0.807	1.602	1.216	0.207	0.207	0.360	1.603	1.188
OPV-Q_{17}A	0.346	1.289	1.580	1.274	0.159	0.101	0.347	1.581	1.262
	0.341	1.356	1.583	1.193	0.189	0.063	0.348	1.582	1.207

Table D4. Parameters retrieved from the analysis of the $I_{VV}(t)$ and $I_{VH}(t)$ decays of metal complex acquired with 20,000 counts at the decay maximum fitted globally when the anisotropy is a monoexponential (aniso01c) and with the triexponential given in Equation 3.19 (aniso02o-3).

	aniso01d-4				aniso02o-3					
Sample	r_0	ϕ (ns)	τ_o (ns)	χ^2	D// (ns-1)	$D_\perp$ (ns-1)	r_0	$<\phi>$ (ns)	τ_o (ns)	χ^2
$OPVQ_4$-Na-Q_4-OPV	0.27	0.83	1.74	1.62	0.09	0.34	0.28	0.83	1.74	1.15
	0.31	0.72	1.73	1.25	1.38	0.34	0.32	0.72	1.73	1.25
	0.34	0.63	1.71	1.15	0.19	0.34	0.34	0.63	1.71	1.23
$OPVQ_8$-Na-Q_8-OPV	0.34	1.25	1.62	1.19	0.10	0.15	0.35	1.36	1.60	1.30
	0.33	1.26	1.61	1.29	0.11	0.15	0.34	1.29	1.61	1.28
$OPVQ_8$-Na-Q_8	0.37	1.21	1.61	1.25	0.13	0.15	0.37	1.20	1.61	1.22
	0.36	1.20	1.62	1.28	0.13	0.15	0.36	1.20	1.62	1.28
$OPVQ_{17}$-Na-Q_8	0.34	1.87	1.60	1.15	0.13	0.06	0.33	1.82	1.62	1.28
	0.34	1.86	1.60	1.27	0.12	0.06	0.34	1.89	1.60	1.25
	0.34	1.79	1.60	1.27	0.13	0.06	0.35	1.86	1.60	1.24
$OPVQ_{17}$-Na-Q_{17}-OPV	0.29	3.08	1.62	1.22	0.09	0.04	0.32	2.58	1.62	1.25
	0.28	3.31	1.62	1.17	0.10	0.04	0.32	2.57	1.62	1.21
	0.28	4.29	1.63	1.18	0.09	0.04	0.33	2.66	1.61	1.29
$OPVQ_{33}$-Na-Q_8	0.30	2.52	1.59	1.18	0.10	0.03	0.32	3.12	1.59	1.20
	0.29	2.59	1.59	1.17	0.10	0.03	0.31	3.10	1.59	1.18
$OPVQ_{33}$-Na-Q_{16}	0.27	2.64	1.63	1.20	0.10	0.02	0.30	3.75	1.62	1.19
	0.28	2.86	1.62	1.25	0.09	0.02	0.31	3.92	1.61	1.22
	0.24	2.68	1.62	1.25	0.11	0.01	0.29	5.34	1.61	1.21

$OPVQ_{33}$-Na-Q_{33}-OPV	0.23	2.75	1.62	1.26	0.09	0.01	0.30	5.82	0.30	1.27
	0.23	2.63	1.62	1.23	0.09	0.01	0.29	5.59	1.60	1.25

Table D5. Parameters of longer metal complexes retrieved from the analysis of the $I_{VV}(t)$ and $I_{VH}(t)$ decays acquired with 20,000 counts at the decay maximum fitted globally when the anisotropy is the function given in Equation 4.17 (aniso03c).

	aniso03c						
Sample	$D_{//}$ (ns^{-1})	$D_{\perp}$ (ns^{-1})	r_0	$<\phi>$ (ns)	τ_o (ns)	*angle*	χ^2
$OPVQ_{33}$-Na-Q_8	0.08	0.03	0.35	0.34	1.59	40	1.15
	0.08	0.03	0.34	3.39	1.59	40	1.16
$OPVQ_{33}$-Na-Q_{16}	0.08	0.02	0.34	4.11	1.62	45	1.15
	0.07	0.02	0.35	4.38	1.61	45	1.19
$OPVQ_{33}$-Na-Q_{33}-OPV	0.07	0.01	0.38	6.26	1.61	60	1.15
	0.06	0.01	0.35	6.74	1.60	45	1.18
	0.06	0.11	0.35	6.77	0.35	50	1.17

E] REFERENCES

1. Siu, H.; Duhamel, J. Global Analysis of the Fluorescence Decays of a Pyrene-Labelled Polymer Using a *Blob* Model. *Macromolecules* **2004**, *37*, 9287-9289.

2. Duhamel, J. New Insights in the Study of Pyrene Excimer Fluorescence to Characterize Macromolecules and their Supramolecular Assemblies in Solution. *Langmuir* **2012**, *28*, 6527-6538.

3. Duhamel, J. Global Analysis of Fluorescence Decays to Probe the Internal Dynamics of Fluorescently Labeled Macromolecules. *Langmuir* **2014**, *30*, 2307-2324.